Integration of recognition, episodic, and associative memories during complex human behavior

Yuchen Xiao[1,11*], Paula Sánchez López[2,3*], Ruijie Wu[4,5*], Peng-Hu Wei[6,7], Yong-Zhi Shan[6,7], Daniel Weisholtz[8], Garth Rees Cosgrove[8], Joseph R Madsen[9], Scellig Stone[9], Guo-Guang Zhao[6,7], Gabriel Kreiman[9,10‡]

[1]Harvard University, Cambridge, MA, USA

[2]Ecole Polytechnique Fédérale de Lausanne, Lausanne, Switzerland

[3]Harvard Medical School, Boston, MA, USA

[4]State Key Laboratory of Brain and Cognitive Science, Institute of Biophysics, Chinese Academy of Sciences, Beijing, China

[5]Hefei Comprehensive National Science Center, Institute of Artificial Intelligence, Hefei, China

[6]Department of Neurosurgery, Xuanwu Hospital, Capital Medical University, Beijing, China

[7]National Center for Neurological Disorders, Beijing, China

[8]Brigham and Women's Hospital, Harvard Medical School, Boston, MA, USA

[9]Boston Children's Hospital, Harvard Medical School, Boston, MA, USA

[10]Center for Brains, Minds and Machines, Cambridge, MA, USA

[11]Current address: Westlake University, Hangzhou, Zhejiang, China

*These authors contributed equally to this work.

[‡]To whom correspondence should be addressed: Gabriel.kreiman@tch.harvard.edu

Author contributions: The task was designed by YX and GK. All the data were collected by RJW (Xuanwu hospital) and YX (BW and BC hospitals) with the help of PHW (Xuanwu) and DW (BWH). GGZ (Xuanwu), YZS (Xuanwu), CRG (BWW), JRM (BCH), and SS (BCH) performed the surgeries on the patients. All the data were curated by YX and analyzed by YX and PSL, with frequent discussions with GK. The manuscript was written by YX, PSL, and GK and approved by all authors.

Competing Interest Statement: The authors have no competing interests.

Classification: Biological Sciences, Neuroscience

Keywords: Episodic memory, human neurophysiology, recognition memory, associative memory, natural behavior

This PDF file includes: Main Text, Figures 1 to 8**,** Table 1

Supplementary material: 12 supplementary figures, 9 supplementary tables

Abstract

The ability to remember what happened where and when constitutes the basic fabric of our memories and who we are. Forming and recalling memories depends on detecting novelty, building associations to prior knowledge, and dynamically retrieving context-relevant information. Previous studies have scrutinized the neural machinery for individual components of recognition or associative memory under laboratory conditions, such as recalling elements from arbitrary lists of words or pictures. In this study, we implemented a well-known card-matching game that integrates multiple components of memory formation together in a naturalistic setting to investigate the dynamic neural processes underlying complex natural human memory. We recorded intracranial field potentials from 1,750 depth or subdural electrodes implanted in 20 patients with pharmacologically-intractable epilepsy while they were performing the task. We leveraged generalized linear models to simultaneously assess the relative contribution of neural responses to distinct task components. Neural activity in the gamma frequency band signaled novelty and graded degrees of familiarity, represented the strength and outcome of associative recall, and finally reflected visual feedback on a trial-by-trial basis. The large-scale data and models enable dissociating and at the same time dynamically tracing the different cognitive components during fast, complex, and natural human memory behaviors.

Significance

Different aspects of memory like recognition, association, and recall have often been studied in isolation under laboratory conditions. Here we implemented a task that naturally integrates recognition, association, and retrieval, mimicking real-world memory experiences. Recording invasive intracranial field potentials from the human brain, this study shows that neural activity in the gamma frequency band in neocortical areas in temporal and frontal cortex reflects temporally overlapping yet computationally dissociable mental processes during dynamic memory formation.

Main Text

Introduction

Episodic memories constitute the essential backbone of our identities. Neural circuits must extract, store, and retrieve information about what, when, and where of specific life events. In stark contrast to most efforts in current artificial intelligence algorithms, the formation and retrieval of episodic memories occurs in a largely unsupervised fashion, with single or limited exposures, and leads to continual learning of new events that are automatically linked to previous experiences. Despite extensive efforts at the molecular, physiological, and behavioral levels, our mechanistic understanding of the formation of episodic memories remains limited.

The formation and recall of memories require assessing novelty versus familiarity, building bridges between sensory inputs and prior knowledge, and effectively retrieving information in the context of current task demands or internal thoughts. There is extensive literature examining neural responses during separate components of this process. A large number of studies have focused on tasks that involve presenting a list of items, such as words, pictures, or video clips, and either recalling items from these lists or assessing recognition memory for those items (e.g., (1-12)). Another prominent experimental paradigm inspired by research in rodents has focused on spatial navigation (e.g., (13-16)).

Judging an item as novel is necessary for its successful memory encoding (17), and recognizing an item as familiar facilitates memory retrieval (18). Several studies have documented correlates of recognition memory for novelty versus familiarity, primarily but not exclusively, in medial temporal lobe structures in rodents, monkeys, and humans (1, 2, 4, 5, 7, 8, 13, 19-23). Both novel and familiar items need to be incorporated into the body of prior knowledge by forming novel associations. Associative memory has been commonly investigated by having participants learn pairs of items and then recall one of the two items or assess whether a given association is correct or not (e.g., (24-33)). Although recognition memory and associative memory have been largely studied separately, they are not independent in real-world memory tasks. Successful implementation of associative memory is contingent on basic recognition processes.

To connect and dissociate different components of memory formation in a natural and complex behavior, here we recorded intracranial field potentials from 20 patients with pharmacologically resilient epilepsy while they played a classical card matching game, colloquially known as the "Memory" game (**Figure 1, Movie S1**). We focused on the neural activities in the gamma frequency band (30-150 Hz), which are thought to indirectly reflect the synchronous firing of ensembles of neurons that support neuronal communication as well as cortical computation (34-38). We constructed generalized linear models to characterize how neural responses are modulated by the different behavioral components involved in the task. The results show how neural circuits transition from representing novelty and graded degrees of familiarity to the strength and outcome of associative recall and reward feedback on a trial-by-trial basis.

Results

We recorded intracranial field potentials (IFPs) from 20 patients with pharmacologically intractable epilepsy implanted with depth electrodes (**Table S1**, one participant also had subdural surface electrodes). Participants played a memory-matching game (**Figure 1, Movie S1, Methods**). Each trial consisted of two self-paced clicks. Clicking on a tile revealed an image (**Figure 1A**). Image categories included person, animal, food, vehicle, and indoor scenes. If the two tiles in a trial contained the same image (*match*, **Figure 1B**), the two tiles turned green and could not be clicked again for the remainder of the block. If the two images were different (*mismatch*, **Figure 1A** and **1C**), the two tiles turned black and could be clicked again. Participants started in a 3×3 tile board block like the one shown in **Figure 1** and progressed to more difficult blocks (4×4, 5×5, 6×6, or 7×7 tiles). All tiles had a corresponding match, except for one tile in the boards with an odd number of tiles (3x3, 5x5, and 7x7).

Mismatch trials showed longer reaction times and were associated with less frequent and less recent exposure to matching pairs

The average number of clicks per tile increased with difficulty (board size), as expected (**Figure 2A**). All participants performed much better than a memoryless model (random clicking, $p<0.001$, here and in subsequent tests unless stated otherwise: permutation test, 5,000 iterations, one-tailed) and performed worse than a model assuming perfect memory ($p<0.001$, **Figure 2A**). The reaction time (RT) was defined as the time interval between the first and second clicks within a trial (**Figure 1A**). The reaction time was longer for mismatch than match trials for all board sizes ($p<0.007$, **Figure 2B**).

For a tile in a given trial, we defined *n-since-last-click* (nslc) as the number of clicks elapsed since the last time *the same tile* was clicked (**Figure 1A**-**B**). As expected, nslc increased with board size ($p<0.001$, linear regression, F-test, **Figure 2C**-**D**). For the 2nd tile, nslc was larger in mismatch compared to match trials for all board sizes except the 3x3 case ($p<0.001$, **Figure 2D**), a reflection of the decay in memory for tiles that were not seen recently. The larger nslc in mismatch trials also held for the 1st tile only for the 7x7 board size ($p<0.001$, **Figure 2C**). If the participants believe that they know the locations of both tiles in a matching pair, a reasonable strategy is to click first the tile they are less sure about, likely because they have seen this tile earlier rather than later in the block. This strategy accounts for the differences between the 1st tile (**Figure 2C**) and 2nd tile (**Figure 2D**).

For a tile in a given trial, we defined *n-since-pair* (nsp) as the number of clicks since the last time when *its matching pair* was seen (**Figure 1A**, **C**). As expected, nsp increased with board size given the increased difficulty ($p<0.001$, linear regression, F-test, **Figure 2E-2F**). Additionally, the more recent the tile's matching pair was seen, the more likely the trial was a match. Thus, nsp was larger in mismatch compared to match trials in all cases except the 3x3 board size for the 1st tile ($p<0.001$, **Figure 2E**). For the 2nd tile, nsp for any match trial was always one because the matching pair would have been revealed in the previous click, by definition. Thus, there was a large difference between nsp between match and mismatch trials ($p<0.001$, **Figure 2F**).

We performed infrared eye-tracking on ten healthy participants while they performed the same task. Participants fixated on the tile they clicked, both for the first and second tiles, and both for match and mismatch trials (**Figure S1**). For the first tile, there was no difference in the dynamics of saccades towards and away from the target tile between match and mismatch trials

149 (**Figure S1A**) after equalizing the RT and the distances between the 1st and the 2nd tiles. For the
150 second tile, there was no difference in the dynamics of saccades toward the target tile before the
151 click. However, for approximately 1 second after the 2nd click, the distance to the center of the
152 tile was, on average, 1.76 dva (degrees of visual angle) larger for match than mismatch trials
153 (**Figure S1B**). This small difference may be attributed to participants' lingering slightly longer
154 during mismatch trials, arguably in an effort to remember the tile.
155
156 **Neural signals reflect novelty and familiarity**
157
158 We recorded intracranial field potentials from 1,750 electrodes (**Table S2**). We excluded
159 582 electrodes due to bipolar referencing, locations in pathological sites, or signals containing
160 artifacts (**Methods**). We included in the analyses 676 bipolarly referenced electrodes in the gray
161 matter (**Figure 3**) and 492 in the white matter (**Figure S2**). **Table S2** describes electrode locations
162 separated by brain region and hemisphere. Although the white matter is presumed to contain
163 mostly myelinated axons, previous studies have shown that intracranial field potential signals
164 from the white matter can demonstrate biologically meaningful information (39, 40). Such signals
165 could reflect small errors in electrode localization on the order of ~2 millimeters and also the
166 spread of intracranial field potential signals over 1 to 5 millimeters (35, 36, 41-43), implying that
167 white matter electrodes may still capture activity from gray matter. Indeed, we show here that
168 electrodes in the white matter reveal task-relevant properties and therefore included electrodes
169 in the white matter in our analyses. To avoid confusion about the origin of the signals, we focused
170 on the gray matter electrodes in the main text and reported results from electrodes in the white
171 matter in the Supplementary Material. None of the conclusions in this study would change if we
172 were to report the results from electrodes in the gray matter exclusively.
173 We built two generalized linear models (GLM) to characterize how the neural responses
174 depended on the cognitive demands of each trial. The first model focused on the neural
175 responses to the 1st tile, and the second model on the 2nd tile. In both cases, we focused on
176 predicting the area under the curve (AUC) of the gamma band power (30-150 Hz) in each trial
177 (**Methods**). For the first GLM, the time window started when the 1st tile was clicked and ended

178 at a time corresponding to the 90th percentile of the distribution of reaction times (time
179 difference between the 1st and the 2nd clicks, **Figure 1A**). This criterion was a reasonable tradeoff
180 between minimizing overlap with responses after the 2nd tile and maximally capturing
181 information before the 2nd tile. For the second model, the time window started with the 2nd click
182 and ended one second afterward.

183 We considered 15 predictors for the GLM models, including whether a trial was a match
184 or not, reaction time, n-since-last-click (nslc), and n-since-pair (nsp), the variables introduced in
185 **Figures 1**-**2**. We also included additional predictors: first-click (whether a tile was clicked for the
186 first time), n-times-seen (number of times an image had been seen), next-match (whether the
187 subsequent trial was a match), board size, x and y position of the clicked tile within the board,
188 distance between the first and the second tiles, and whether the image contained a person,
189 animal, food, or vehicle. **Table 1** lists all the predictors and their definitions. Since several
190 predictors were correlated with each other (**Figure S3A**-**B**), we computed the variance inflation
191 factor (VIF) (44), a metric commonly used to account for correlations between predictors in
192 generalized linear models. The VIF of each predictor was smaller than 3 for all participants (**Figure**
193 **S3C**-**D**). Therefore, the correlations between predictors did not harm the performance of the
194 models (**Methods**).

195 When the first tile in a trial was clicked, its status in memory guided the following actions.
196 If it was a new image, the participant needed to encode it in memory for future retrieval. Thus,
197 the ability to detect novelty is the first step for successful encoding. The predictor *first-click*
198 described novelty and had a value of 1 whenever a tile was seen for the first time and 0 otherwise.
199 If a tile had been viewed before, it would appear familiar to the participant, and the degree of
200 familiarity depended on how long ago that tile had been seen last. The predictor n-since-last-click
201 (**Figure 1A**-**B, Figure 2C**-**D**) described familiarity; the smaller nslc, the more familiar the tile is
202 because that same tile was seen more recently.

203 **Figure 4A**-**D** shows the neural activity of an electrode located in the right lateral
204 orbitofrontal cortex (arrow in **Figure 4D**), whose responses to the first tile correlated with novelty.
205 The GLM analysis indicated that first-click was a significant predictor of the neural responses
206 (**Figure 4A**). The neural responses to the first tile showed a decrease in activity for novel tiles

207 compared to tiles that had been seen before (**Figure 4B**), which could also be readily seen in
208 individual trials (**Figure 4C**). This decrease in activity is reflected by the negative sign in the GLM
209 first-click predictor (**Figure 4A**).

210 Novelty was a significant predictor of the neural responses after the first tile ($p<0.01$, GLM)
211 for 50 electrodes in the gray matter (7.4% of the total, **Table S3A**, **Figure 4D**) and 33 electrodes
212 in the white matter (6.7% of the total, **Table S3B**). The lateral orbitofrontal (LOF) cortex and pars
213 opercularis contained significantly more electrodes than expected by chance ($p<0.01$, **Methods**).

214 **Figure 4E-H** show the neural activity of an electrode located in the left pars opercularis
215 (arrow in **Figure 4H**), whose responses to the first tile correlated with familiarity. The GLM
216 analysis indicated that both n-since-last-click (nslc) and first-click were significant predictors of
217 the neural responses ($p<0.001$, GLM, **Figure 4E**). Novel tiles (completely unfamiliar tiles, **Figure**
218 **4F**, blue) elicited strong responses, followed by less familiar tiles (higher nslc, **Figure 4F**, yellow).
219 Familiar tiles (nslc=1, i.e., tiles that had just been seen in the preceding trial) elicited almost no
220 response (**Figure 4F**, red). The strong correlation between the neural responses, novelty, and
221 familiarity can also be readily appreciated in individual trials (**Figure 4G**).

222 The reaction time was also a significant predictor for the neural responses recorded from
223 this electrode (**Figure 4E**). However, the differences in neural responses signaling novelty and
224 distinct degrees of familiarity *cannot* be explained by differences in reaction time. The differences
225 in neural responses associated with novelty and familiarity persisted after reaction time
226 equalization (see vertical dashed lines indicating equalized RT in **Figure 4F**).

227 The nslc predictor was statistically significant ($p<0.01$, GLM) in 45 gray matter electrodes
228 (6.7% of the total, **Table S4A**, **Figure 4H**) and 32 white matter electrodes (6.5%, **Table S4B**, **Figure**
229 **S4D**). **Figure S4** shows an example electrode located in the white matter whose responses
230 correlated with novelty and familiarity. The majority of electrodes (82.2%) showed a positive
231 correlation between the neural responses and nslc as illustrated in **Figure 4E-G**. The remaining
232 electrodes (17.8%) showed a negative correlation, i.e., stronger neural responses for more
233 familiar items. **Figure S5** depicts an example electrode located in the right pars opercularis
234 showing a negative correlation between familiarity and neural responses.

235 Both the electrode in **Figure 4E-H** and the one in **Figure S5** revealed first-click as a
236 significant predictor in addition to nslc, meaning that their responses not only reflected the
237 familiarity gradient but also represented novelty. The electrodes that showed both first-click and
238 n-since-last-click as significant predictors (20 electrodes) are denoted by red circles in **Figure 4D**
239 and **Figure 4H**. Among these 20 electrodes, the signs of the t-statistic for the first-click and n-
240 since-last-click predictors were consistent for 18 electrodes (16 positive and 2 negative). Only
241 two electrodes exhibited opposite signs. These results indicate that novelty largely resembles
242 extremely low familiarity in terms of the underlying neural responses.
243
244 **Neural signals predict correct retrieval**
245
246 After seeing the 1st tile, participants attempt to find the tile's pair. If the 1st tile's pair was
247 never encountered before, this is a random choice among the unseen tiles. If the tile's pair is
248 unfamiliar, recalling a match is error-prone and often leads to mismatches (**Figure 2E**). For highly
249 familiar cases, participants can retrieve the correct location to find the match tile. Therefore, we
250 asked whether the neural responses after exposure to the first tile and before seeing the 2nd tile
251 could predict successful retrieval.
252 **Figure 5** shows the neural activity of an electrode located in the right lateral orbitofrontal
253 cortex (arrow in **Figure 5E**), whose responses were predictive of successful retrieval. The GLM
254 analysis indicated that match was a significant predictor of the neural responses ($p<0.001$, **Figure**
255 **5A**). This electrode showed stronger responses during match trials (**Figure 5B**, green) than during
256 mismatch trials (**Figure 5B**, black). These differences can even be appreciated in single trials
257 (compare **Figure 5C** versus **Figure 5D**). Of note, these differences are evident shortly after
258 visualization of the first tile, with a peak at 500 ms after clicking the first tile, well before clicking
259 the second tile, when the participant did not know for certain yet whether the trial would be a
260 match or not. Thus, the strong neural differences between match and mismatch trials reflect the
261 participant's internal retrieval of the correct pairs' locations.
262 Whether a trial was a match or not was a significant predictor of the neural responses for
263 32 electrodes in the gray matter (4.7% of the total, **Table S5A**, **Figure 5E**) and 30 electrodes in

264 the white matter (6% of the total, **Table S5B**, **Figure S6**). For an example electrode in the white
265 matter see **Figure S6**. In most cases (91 %), neural activity was higher during match trials than
266 during mismatch trials, as illustrated in **Figure 5**. The locations of all these electrodes, shown in
267 **Figure 5E** (gray matter) and **Figure S6** (white matter), reveal that the majority were located in the
268 lateral orbitofrontal (LOF) cortex, the medial temporal lobe, and the insula. The LOF cortex
269 contained significantly more electrodes than expected by chance ($p<0.01$, **Methods**).

270 The peak in neural activity occurred at approximately 500 ms after the 1st click (**Figure 5B**).
271 As discussed in the previous section, the match predictor correlated with several other predictors
272 (**Figure S3**). However, the GLM analysis shows that the match's presence, but not other
273 predictors, accounts for the neural responses (**Figure 5A**). To further establish this point, **Figure**
274 **S7A** shows the responses of this same electrode, in the same format as **Figure 5B**, after equalizing
275 the n-since-last-click (nslc) distributions for match and mismatch trials by subsampling the data.
276 The same conclusions hold in this case. Furthermore, **Figure S7B** shows each match trial's gamma
277 power AUC versus the value of n-since-last-click and **Figure S7C** displays the same data from
278 mismatch trials. The variable nslc did *not* account for the neural responses in either case ($p>0.18$,
279 linear regression). Similar conclusions hold for the other predictors.

280 **Figure S8** shows another example electrode located in the left middle temporal gyrus
281 where the match was a significant predictor for the gamma band activity between the 1st and 2nd
282 tiles. Similar to the LOF electrode in **Figure 5**, the gamma power during match trials was higher
283 than during mismatch trials. However, the pattern of modulation in this electrode was sustained
284 rather than transient (compare **Figure S8** versus **Figure 5B**-**D**). The change in gamma power was
285 also evident in individual trials (**Figure S8B**-**C**). These observations suggest that the middle
286 temporal and lateral orbitofrontal regions might be functionally distinct during memory retrieval.
287 In sum, these results indicate that even before the actual realization of whether a trial was a
288 match or mismatch (i.e., before the onset of the 2nd tile), there were distinct neural responses
289 that were predictive of the trial's outcome.

290

291 **Neural signals reflect the strength of memory retrieval**

292

In addition to reflecting the outcome of a given trial (match versus mismatch), we considered the *n-since-pair* (nsp) predictor as a proxy for the degree of confidence or strength of memory retrieval. The smaller nsp, the more recently *the tile's pair* had been seen (**Figure 2E-F**). This predictor is different from n-since-last-click, which indicates how recently *the same tile*, rather than its pair, had been seen (**Figure 1**). We considered only match trials for this predictor (n-since-pair*match) because there was no successful retrieval of the tile's pair in mismatch trials.

Figure 6 shows an example electrode in the left middle temporal gyrus (arrow in **Figure 6E**). In contrast with the electrode in **Figure 5**, both the match predictor and the nsp predictor were significant in the GLM analysis (**Figure 6A**). The t-statistic for nsp was negative, indicating a *decrease* in gamma band power for matching pairs that were more distant in memory. Indeed, responses were strongest for those tiles whose pairs had been seen less than 2 clicks ago (**Figure 6B**, red) and weakest when matching pairs had been seen more than 10 clicks ago (**Figure 6B**, purple). There was a negative correlation between the area under the curve (AUC) of the gamma band power and nsp (**Figure 6C**, $p<0.001$, linear regression). This correlation disappeared when considering mismatch trials (**Figure 6D**, $p=0.66$, linear regression), suggesting that the relationship between the neural signals and memory strength was contingent on successful retrieval.

The nsp predictor was statistically significant ($p<0.01$, GLM) in 15 electrodes in the gray matter (2.2% of the total, **Table S6A**, **Figure 6E**) and 9 electrodes in the white matter (1.8% of the total, **Table S6B**, **Figure S9E**). For an example electrode located in the white matter, see **Figure S9**. Most of these electrodes showed a negative t-statistic, as in the example in **Figure 6**, and three electrodes (20%) showed the reverse effect (i.e., an increase in the neural signal for more distant associative memories). For most of these electrodes (73.3%), *match* was also a significant predictor, as illustrated by the example in **Figure 6A**, indicating that the neural signals encoded *both* successful retrieval *and* memory strength.

Neural signals reflect feedback after the second tile

321 We have thus far focused on describing the responses elicited by the first tile in each trial.
322 Next, we evaluated the neural responses triggered by the click of the second tile. We first asked
323 whether novelty and familiarity were also encoded in the neural responses after the 2nd tile. We
324 built a separate GLM using the same 15 predictors except for n-since-pair*match (**Table 1**) to
325 describe the AUC of the gamma power during one second after clicking the 2nd tile. We excluded
326 n-since-pair*match here because it would always be 1 during match trials (by definition, the first
327 click was the pair of the second click). For the second tile, first-click was a significant predictor in
328 24 electrodes in the gray matter (3.6% of the total, **Table S7A**, **Figure S10E**) and 12 in the white
329 matter (2.4% of the total, **Table S7B**). Thus, less than half the number of electrodes reflected
330 novelty during the 2nd tile compared to the first tile (cf. **Table S7A** versus **Table S3A** and **Table**
331 **S7B** versus **Table S3B**). For the second tile, *n-since-last-click* was a significant predictor in 9
332 electrodes in the gray matter (1.3% of the total, **Table S8A**, **Figure S10D**) and 24 in the white
333 matter (4.9% of the total, **Table S8B**), again, less than half the number of electrodes reflecting
334 familiarity during the first tile (cf. **Table S8A** versus **Table S4A** and **Table S8B** versus **Table S4B**).
335 An example electrode in the LOF region whose responses correlated with familiarity after
336 the 2nd tile is shown in **Figure S10**. The LOF cortex contained significantly more electrodes than
337 expected by chance ($p<0.01$, **Methods**). Among all the 9 electrodes where n-since-last-click was
338 a significant predictor during the 2nd tile, 7 electrodes also had first-click as a significant predictor
339 (**Figure S10D-E**, red circles). In sum, novelty and familiarity of a tile were still encoded in the
340 neural responses to the second tile, but to a lesser degree than during the responses to the first
341 tile. This reduction may be due to the fact that two images were presented simultaneously, and
342 the neural signals might reflect a weighted combination of the responses to each (45). Moreover,
343 for match trials, the information about the 2nd tile does not need to be encoded in memory
344 anymore to thrive in the task.
345 Among the 83 electrodes that had first-click as a significant predictor during the 1st tile
346 and the 36 electrodes during the 2nd tile (including both gray and white matter), 15 electrodes
347 (11 gray matter + 4 white matter) overlapped, i.e., first-click was a significant predictor during
348 both the 1st and the 2nd tiles. Among the 77 electrodes that had n-since-last-click as a significant
349 predictor during the 1st tile and the 33 electrodes during the 2nd tile (including both gray and

350 white matter), 20 electrodes (5 gray matter + 15 white matter) overlapped, i.e., nslc was a
351 significant predictor during both the 1st and the 2nd tiles. These electrodes may reflect general
352 rather than specific novelty or familiarity mechanisms, irrespective of tile order, image content,
353 or location.

354 Next, we asked whether the differences between match and mismatch trials were also
355 manifested *after* the 2nd tile was revealed, i.e., after the participant became explicitly aware of
356 whether the trial was a match or not. **Figure 7** shows an example electrode located in the left
357 insula (see arrow in **Figure 7E**) where match was a significant predictor for the neural responses
358 after the 2nd tile ($p<0.001$, GLM, **Figure 7A**). The neural signals during match trials were larger
359 than during mismatch trials (**Figure 7B**) and could be readily observed even in single trials (**Figure**
360 **7C** vs. **7D**).

361 After the 2nd tile, the match predictor was statistically significant ($p<0.01$, GLM) for 112
362 electrodes in the gray matter (16.6% of the total, **Table S9A**, **Figure 7E**) and 66 electrodes in the
363 white matter (13.4% of the total, **Table S9B**, **Figure S11E**). For an example electrode in the white
364 matter, see **Figure S11**. The locations of all these electrodes, shown in **Figure 7E** (gray matter)
365 and **Figure S11E** (white matter), reveal that the majority were circumscribed to the LOF and the
366 insula. The proportions of significant electrodes in both regions were higher than expected by
367 chance ($p<0.01$, **Methods**).

368 There were 17 electrodes in the gray matter and 15 in the white matter where the match
369 predictor was significant for both the 1st and the 2nd tiles. These electrodes represented 53.1%
370 (gray matter) and 50% (white matter) of the electrodes that were significant according to the 1st
371 tile, and 15.2% (gray matter) and 22.8% (white matter) of the electrodes that were significant
372 according to the 2nd tile. These electrodes were located in the lateral orbitofrontal cortex, the
373 medial temporal lobe, and the insula (**Figure 5E**, **S6E**, **7E**, and **S11E**, red circles). The electrode in
374 **Figure S11** exemplifies such electrodes. The electrode in **Figure S8** reveals a continuous
375 enhancement for match trials after the 1st tile that was sustained and continued after the onset
376 of the 2nd tile.

377

378 **A machine learning classifier could predict matches in single trials**

We evaluated whether the neural responses within a brain region could predict if a trial was a match or a mismatch (**Methods**). For this analysis, we considered only those brain regions with more than 12 electrodes combining all participants (**Methods**). **Figure 8** shows the average decoding performance of an SVM classifier after 200 iterations of 5-fold cross-validation. At each iteration, the SVM consisted of a binary classifier (match versus mismatch). The predictors were the PCA features extracted from the concatenated neural responses of electrodes within a particular brain region. The superior parietal gyrus and insula exhibited decoding accuracy above chance ($p<0.01$, **Methods**) during the 1st tile (**Figure 8A**). The lateral orbitofrontal and middle temporal cortex also showed accuracy above chance (>60%, **Figure 8A**), albeit not statistically significant. As expected based on the responses of individual electrodes, the decoding accuracy was higher after the 2nd tile compared to the 1st tile. After the 2nd tile, multiple brain regions showed accuracy above chance ($p<0.01$, **Figure 8B**). The lateral orbitofrontal cortex, insula, middle temporal gyrus, and pars opercularis showed the highest accuracy (>75%). Similar results were obtained when subsampling 12 electrodes during each iteration (**Figure S12**).

Discussion

In this study, we followed the dynamics of neural signals during a natural memory task based on a classical card-matching game. Participants performed the task very well, slightly worse than expected by a perfect memory model (**Figure 2A**), showing increased reaction times during mismatch trials (**Figure 2B**) as well as decay of memory traces with time since encoding (**Figure 2C-F**). The extensive sampling of brain regions afforded by studying the neural activity of more than 1,000 electrodes across 20 participants (**Figure 3** and **Figure S2**) enabled us to track neural responses during each of the steps required in the task with broad brain coverage.

The first step to encode tile information is to correctly determine whether a tile is novel or not. We refer to the ability to detect novelty and familiarity as non-associative recognition memory (6, 27). Assessment of novelty and familiarity orchestrate encoding and maintenance strategies (17, 46). We found strong neural responses that signal novelty and familiarity (**Figure**

408 **4**, **Figure S4, S5** and **S10**, **Table S3, S4, S7** and **S8**). Several electrodes responded both to novelty
409 and familiarity. In these cases, novel and highly unfamiliar items triggered similar neural
410 responses (**Figure 4F-G**, **Figure S4B-C**, **Figure S10B-C**). The lateral orbitofrontal cortex, the pars
411 opercularis, and the medial temporal lobe contained a preponderance of electrodes signaling
412 novelty and familiarity. These responses are reminiscent of novelty and familiarity signals that
413 have typically been described in tasks involving a sequence of images presented with occasional
414 repetitions (6, 7, 10, 47) but are not restricted to the medial temporal lobe. While some
415 electrodes may also encode information about the image content (**Figure 4E**), the fact that
416 correlates of familiarity can be observed at the level of intracranial field potentials suggests that
417 the representation of familiarity may not be content-specific. Different contents with the same
418 level of familiarity may induce the same response, consistent with the observation that neurons
419 involved in memory formation are rarely sharply tuned to particular sensory features (31).

420 After seeing the first tile in a trial, participants could estimate whether they remembered
421 the location of its pair and, thus, whether they would get a match or not. Participants link the
422 first tile with its pair to internally predict where to click next. Indeed, neural responses strongly
423 reflected not only these predictions (**Figure 5**, **Figures S6**, **S8**) but also the internal estimate of
424 the strength or the confidence of these predictions (**Figure 6**). Even though participants could not
425 know for sure yet whether the trial would be a match or not, the neural signals demonstrated a
426 large difference between match and mismatch trials after the first tile and before the revelation
427 of the second tile. These differences were either transient (**Figure 5**) or sustained (**Figure S8**). We
428 speculate that transient increases in activity during match trials might signal the sudden
429 realization and high confidence about the trial outcome (match or mismatch). In contrast,
430 sustained responses may correspond to the active retrieval processes. It is possible that sustained
431 activity could arise due to averaging across temporally shifted transient activities from individual
432 neurons (48). However, it has been reported that single neurons in the hippocampus can also
433 show sustained firing rate increase for successful associative retrieval (49). Extensive work has
434 documented the importance of the hippocampus and surrounding structures in the MTL in
435 associative memory (e.g., (6, 29, 49, 50)). In addition to the MTL, the current results show that
436 other areas, such as the lateral orbitofrontal cortex, also play a critical role in associative recall.

Many studies have focused on studying memory for a list of sequentially presented words, images, or other stimuli (5, 11, 17, 21, 27, 47, 51). Other studies have examined memory formation in naturalistic or real-world scenarios at the behavioral level (52-56). The task introduced here is in between these two extremes. The card-matching game is more realistic and adds multiple complexities compared to a sequence of individual images or words. Yet, it allows for a high level of control over stimulus timing and experimental parameters that are difficult to achieve when studying memory in real-world scenarios. The neurophysiological responses tracked multiple steps in the task, from detecting novel tiles to their subsequent encoding, association, retrieval, and feedback.

Complex and natural tasks necessarily depend on the interplay of multiple intercorrelated variables. To tame the complexity of these different variables, we used generalized linear models to quantitatively assess the influence of distinct predictors on the neural responses. Through these GLM analyses, we could characterize neurophysiological responses that were largely governed by individual predictors after accounting for the correlations among predictors (**Figure S3**). While focusing on any one predictor, these results were corroborated by subsampling the data to equalize other predictor variables that potentially affect the neural responses. Given the complexity of the task and the nature of the intracranial field potential signals studied here, it is remarkable that it is possible to isolate individual aspects of the task reflected in the neurophysiological responses.

The high temporal resolution, extensive spatial sampling, and systematic computational models provide an opportunity to characterize the dynamics of complex naturalistic tasks. These observations provide initial steps to further our understanding of how different components of encoding and retrieval interact during the formation of natural memory events.

Methods

Task paradigm

Participants performed our implementation of the classical memory matching game (**Figure 1, Movie S1**). The game involves remembering the location and content of a set of tiles

466 to find all the matching pairs. A square board containing $n \times n$ tiles was shown throughout each
467 block. In the beginning, all tiles were shown in black. In each trial, participants chose one tile, and
468 then a second tile, by clicking on them in a self-paced fashion. Upon clicking, the tile revealed a
469 common object like a cat or an indoor scene like a kitchen. At the end of each trial, either the
470 two tiles revealed the same content (match) or not (mismatch). If the tiles matched, then the two
471 tiles turned green 1,000 ms after the second click, and the two tiles could not be clicked again for
472 the remainder of the block. If the tiles did not match, they turned black 1,000 ms after the second
473 click and could be clicked again in subsequent trials. When all tiles turned green, i.e., all matches
474 were found, the block ended, and another block began. During each block, the map between
475 positions and objects was fixed. The game always started with a block of size 3×3 and progressed
476 to more difficult blocks (4×4, 5×5, 6×6, and finally 7×7). Blocks with an odd number of tiles (3×3,
477 5×5, and 7×7) contained one distractor object (a human face) with no corresponding pair. For
478 each block except the 3×3 board, there was a limit for the total time elapsed (2 minutes for 4×4,
479 3.3 min for 5×5, 4.8 min for 6×6, and 8.2 min for 7x7). If a participant did not complete a block
480 within the time limit, the block ended, and a new, easier block started by reducing the board size
481 n by 1, except when n=7, where it was reduced by 2. Conversely, when participants successfully
482 completed a block with a board of size n within the allotted time limit, they moved on to a more
483 difficult block by increasing n by 1. When participants completed an n=7 block, they performed
484 further n=7 blocks. There was no image repetition across blocks.
485 All the images were from the Microsoft COCO 2017 validation dataset (57) and were
486 rendered in grayscale and square shape. We included a balanced number of pictures from 5
487 categories: person, animal, food, vehicle, and indoor scenes. All the images were rendered on a
488 13-inch Apple MacBook Pro laptop. The size of each tile was 0.75×0.75 inches (approximately 2x2
489 degrees of visual angle, dva) and the separation between two adjacent tiles was 0.125 inch (0.33
490 dva) for board size n=7 and 0.25 inch (0.67 dva) for the others. The game implementation was
491 written and presented using the Psychtoolbox extension (58, 59) in Matlab_2016b (Mathworks,
492 Natick, MA).
493
494 **Epilepsy participants and recording procedures**

We recorded intracranial field potentials from 20 patients with pharmacologically intractable epilepsy (12-52 years old, 9 female, **Table S1**) undergoing monitoring at Boston Children's Hospital (Boston, US), Brigham and Women's Hospital (Boston, US), and Xuanwu Hospital (Beijing, China). All recording sessions were seizure-free. All patients had normal or corrected-to-normal vision. The study protocol was approved by each hospital's institutional review board. Experiments were run under patients' or their legal guardians' informed consent. One patient at Brigham and Women's Hospital (BWH) was implanted with both stereo encephalography (sEEG) and electrocorticography (ECoG) electrodes, while all other patients had only sEEG electrodes (Ad-tech, USA; ALCIS, France). Intracranial field potentials were recorded with Natus (Pleasanton, CA) and Micromed (Italy). The sampling rate was 2048 Hz at Boston Children's Hospital, 512 Hz or 1024 Hz at BWH, and 512 Hz at Xuanwu Hospital. Electrode trajectories were determined based on clinical purposes for precisely localizing suspected epileptogenic foci and surgically treating epilepsy (60).

Eye tracking procedures

Ten non-epilepsy healthy participants (23-35 years old, 9 female) performed the same task while their eye movements were tracked with the EyeLink 1000 plus system (SR Research, Canada) at a sampling rate of 500 Hz. The task paradigm was the same as the one for epilepsy participants except that, before each block began, participants fixated on a center cross to ensure that the EyeLink eye-tracking system was well-calibrated. Otherwise, a re-calibration session ensued. The task was presented on a 19-inch CRT monitor (Sony Multiscan G520), and participants sat about 21 inches away from the monitor screen. The tile size was 1x1 inches (approximately 2.7x2.7 degrees of visual angle) as appeared on the screen. The study protocol was approved by the institutional review board at Boston Children's Hospital, and each participant completed the task with informed consent. All participants had normal or corrected-to-normal vision. All participants completed 16 blocks.

Behavioral analyses

We created two computational models to simulate behavior assuming perfect memory or no memory (chance performance, **Figure 2A**). The perfect memory model remembered all revealed tiles without forgetting. The random model simulated random clicking. We calculated the reaction time (RT, time between two clicks in a trial), n-since-pair (number of clicks since the last time when a tile's matching pair was seen), n-since-last-click (the number of clicks since the same tile was clicked), and n-times-seen (number of times the same image had been seen). For n-since-pair and n-since-last-click, we excluded trials in which any tile was seen for the first time, i.e., when a tile's matching pair had never been revealed, or there was no previous click. We compared these variables for match and mismatch trials at each board size (**Figure 2**, permutation test, 5,000 iterations, α=0.01). We defined random matches as a match trial where the second tile had never been seen before; such trials were excluded from both the behavioral and neurophysiological analyses. We used the F-test for linear regression models to assess whether RT, n-since-pair, n-since-last-click, and n-times-seen significantly covary with board size. The linear regression models' predictors were these four behavioral parameters and the dependent variable the board size. We created separate models for match and mismatch trials and 1st and 2nd tiles.

Electrode localization

Electrodes were localized using the iELVis (61) toolbox. We used Freesurfer (62) to segment the preimplant magnetic resonance (MR) images, upon which post-implant CT was rigidly registered. Electrodes were marked in the CT aligned to preimplant MRI using Bioimage Suite (63). Each electrode was assigned to an anatomical location using the Desikan-Killiany (64) atlas for subdural grids or strips or FreeSurfer's volumetric brain segmentation for depth electrodes. For white matter electrodes, we also reported their closest gray matter locations. Out of 1,750 electrodes in total, we included 676 bipolarly referenced electrodes in the gray matter (**Figure 3, Table S2**) and 492 bipolarly referenced electrodes in the white matter (**Figure S2, Table S2**). Five hundred eighty-two electrodes were not considered for analyses due to bipolar referencing, locations in pathological sites, or electrodes containing large artifacts. Electrode

551 locations were mapped onto the MNI305 average brain via affine transformation (65) for display
552 purposes (e.g., **Figure 3**).
553
554 **Preprocessing of intracranial field potential data**
555 Bipolar subtraction was applied to each pair of neighboring electrodes on each shank of
556 depth electrodes or subdural grids/strips (66). A zero-phase digital notch filter (Matlab function
557 "filtfilt") was applied to the bipolarly subtracted broadband signals to remove the line frequency
558 at 60 Hz (BCH, BWH) or 50 Hz (Xuanwu) and their harmonics. For each electrode, trials whose
559 amplitudes ($Voltage_{max}$-$Voltage_{min}$) were larger than 5 standard deviations from the mean
560 amplitude across all trials were considered potential artifacts and discarded from further
561 analyses (67). For the first tile, the time window for artifact rejection was from 400 ms before the
562 click until 1 second after the average RT. For the second tile, the time window was [400 ms +
563 average RT] before the second click until 1 second after the second click. Across all electrodes,
564 we rejected 1.75% of all trials for the 1st tile and 1.73% for the second tile.
565
566 **Time-frequency decomposition**
567 The gamma band (30-150 Hz) power was computed using the Chronux toolbox (68). We
568 used a time-bandwidth product of 5 and 7 leading tapers, a moving window size of 200 ms, and
569 a step size of 10 ms (69). For each trial, the power was normalized by subtracting the mean
570 gamma band power during the baseline (400 ms before 1st tile) and dividing by the standard
571 deviation of the gamma power during the baseline. For all the participants, there were more
572 mismatch than match trials. In the raster plots, we subsampled the mismatch trials, keeping
573 those trials whose reaction times were closest to the mean reaction time of match trials. All
574 random matches were excluded from analyses.
575
576 **Generalized linear model**
577 We used generalized linear models (GLM) (70, 71) to analyze the relationship between
578 the gamma band power and behavioral parameters. We used two different GLMs, one using
579 neural responses between the 1st and the 2nd tiles and the other using neural responses after the

580 2nd tile. For the first GLM, the time window started when the 1st tile was clicked and ended at a
581 time corresponding to the 90th percentile of the distribution of reaction times (time difference
582 between the 1st and the 2nd click, **Figure 1A**) for each participant. This criterion was a reasonable
583 tradeoff between minimum overlap with responses after the 2nd tile and the maximum amount
584 of information captured. For the second GLM, we used 1 second after the 2nd tile click as the
585 analysis window. The response variable to be fit by the GLM analyses was defined as the area
586 under the curve (AUC) of the gamma band power over the specified time windows. **Table 1**
587 describes the behavioral parameters that were considered as predictors in the models.

588 We performed a multicollinearity analysis to assess the presence of highly correlated
589 predictors that could impair the model's performance (72, 73). We calculated the variance
590 inflation factor (VIF) for each predictor to detect the presence of multicollinearities. A VIF of 1
591 indicates that there is no correlation with other predictors. The larger the VIF, the higher the
592 correlation. A VIF greater than 5 indicates a very high correlation that could significantly harm
593 the model's performance. For all participants in our analysis, the VIFs of all predictors were
594 smaller than 3 (**Figure S3C-D**).

595 For n-since-pair, we included the interaction term between this predictor and match (n-
596 since-pair*match) to test the hypothesis that when a trial was a match, the strength of the neural
597 response after the first tile was modulated by how recently the tile's matching pair was seen for
598 the last time. The neurophysiological responses confirmed that this is a reasonable way to model
599 the data (**Figure 6B**). We represented image categories as predictor variables in the GLM by
600 including four out of the five categories (animal, food, vehicle, and person). We dropped the
601 "indoor" category to avoid falling into the "dummy variable trap" (74). For each predictor, we
602 calculated the parameter estimate (beta coefficient) from the least mean squares fit of the model
603 to the data, the t-statistic (beta divided by its standard error), and the p-value to test the effect
604 of each predictor on the neural responses. A beta coefficient or t-statistic of zero indicated that
605 the predictor did not affect the neural responses. A predictor was considered statistically
606 significant if the GLM model differed from a constant model ($p<0.01$) and the p-value for that
607 predictor was smaller than 0.01.

To determine if any brain region contained significantly more electrodes than expected by chance considering any GLM predictor, we randomly sampled the same number (n) of electrodes as those where that predictor was significant, from the total electrode population (separately for gray and white matter electrodes) for 5,000 iterations. Taking the *match* predictor for gray matter electrodes as an example, from the total of 676 gray matter electrode locations, we randomly sampled 32 electrodes (the number of match-significant gray matter electrodes) 5,000 times, and calculated the p-value of any location, say insula, as the number of times when n for insula and match-significant was less than n for insula sampled. If $p<0.01$, that brain region was considered to have significantly more electrodes than expected by chance.

Decoding of match

We used a machine learning decoding approach to evaluate whether the neural responses from a given brain region could predict whether the trial was a match or a mismatch. For this analysis, we selected only those brain regions in which we had at least 12 electrodes. We used two different decoders for each brain region, one using neural responses between the 1st tile and 800 ms after the 1st tile click, and the other using the neural responses between the 2nd tile and 800 ms after the 2nd tile click. We performed 200 iterations of 5-fold cross-validation for each brain region and tile to split the trials into independent train and test sets (1,000 splits in total). We concatenated the neural responses of electrodes within the same brain region, using two different approaches: (i) taking all electrodes in each brain region, and (ii) randomly subsampling 12 electrodes at each iteration. The number of match and mismatch trials was normalized by random subsampling. To reduce the dimensionality of the neural responses, we used principal component analysis (PCA). The PCA parameters were computed using only the training data, and we selected the number of components that could explain 70% of the training neural responses variance. We used support vector machines (SVM) with a linear kernel for the binary classification (match or mismatch), using as the model inputs the PCA features computed from the neural responses. We followed the same procedure to test whether the classification performance was above chance, but we randomized the response variable (match or mismatch) at every iteration. We calculated the p-value as the number of times when the accuracy using

random labels was above the average accuracy using the actual labels. If $p<0.01$, neural responses of that brain region could predict match and mismatch above chance.

Data availability

We share all the deidentified psychophysics data, electrode location information, and neural data, together with all the code generated to model and analyze the data through the following public site: https://klab.tch.harvard.edu/resources/HowToGetAMatch.html

Acknowledgments

This work was supported by the McKnight Foundation, NIH Grant R01026025, and NSF Grant CCF-1231216.

References

1. S. M. Daselaar, M. S. Fleck, R. Cabeza, Triple dissociation in the medial temporal lobes: recollection, familiarity, and novelty. *J Neurophysiol* **96**, 1902-1911 (2006).
2. I. Fried, K. A. MacDonald, C. Wilson, Single neuron activity in human hippocampus and amygdala during recognition of faces and objects. *Neuron* **18**, 753-765 (1997).
3. J. Zheng *et al.*, Neurons detect cognitive boundaries to structure episodic memories in humans. *Nature Neuroscience* **25**, 358-368 (2022).
4. R. J. Murray, T. Brosch, D. Sander, The functional profile of the human amygdala in affective processing: insights from intracranial recordings. *Cortex* **60**, 10-33 (2014).
5. I. V. Viskontas, B. J. Knowlton, P. N. Steinmetz, I. Fried, Differences in mnemonic processing by neurons in the human hippocampus and parahippocampal regions. *J Cogn Neurosci* **18**, 1654-1662 (2006).
6. U. Rutishauser, Testing Models of Human Declarative Memory at the Single-Neuron Level. *Trends Cogn Sci* **23**, 510-524 (2019).
7. M. A. Yassa, C. E. Stark, Multiple signals of recognition memory in the medial temporal lobe. *Hippocampus* **18**, 945-954 (2008).
8. T. Zaehle *et al.*, Nucleus accumbens activity dissociates different forms of salience: evidence from human intracranial recordings. *J Neurosci* **33**, 8764-8771 (2013).
9. E. L. Johnson, R. T. Knight, Intracranial recordings and human memory. *Curr Opin Neurobiol* **31**, 18-25 (2015).
10. R. Knight, Contribution of human hippocampal region to novelty detection. *Nature* **383**, 256-259 (1996).
11. P. B. Sederberg *et al.*, Hippocampal and neocortical gamma oscillations predict memory formation in humans. *Cereb Cortex* **17**, 1190-1196 (2007).

12. H. L. Roediger, 3rd, E. Tekin, Recognition memory: Tulving's contributions and some new findings. *Neuropsychologia* **139**, 107350 (2020).
13. J. Park *et al.*, Role of low- and high-frequency oscillations in the human hippocampus for encoding environmental novelty during a spatial navigation task. *Hippocampus* **24**, 1341-1352 (2014).
14. J. Jacobs *et al.*, Right-lateralized Brain Oscillations in Human Spatial Navigation. *J Cogn Neurosci* 10.1162/jocn.2009.21240 (2009).
15. A. D. Ekstrom *et al.*, Cellular networks underlying human spatial navigation. *Nature* **425**, 184-187 (2003).
16. Z. Aghajan *et al.*, Theta Oscillations in the Human Medial Temporal Lobe during Real-World Ambulatory Movement. *Curr Biol* **27**, 3743-3751 e3743 (2017).
17. E. Tulving, N. Kroll, Novelty assessment in the brain and long-term memory encoding. *Psychon Bull Rev* **2**, 387-390 (1995).
18. K. D. Duncan, D. Shohamy, Memory states influence value-based decisions. *J Exp Psychol Gen* **145**, 1420-1426 (2016).
19. D. Montaldi, T. J. Spencer, N. Roberts, A. R. Mayes, The neural system that mediates familiarity memory. *Hippocampus* **16**, 504-520 (2006).
20. V. Mehrpour, T. Meyer, E. P. Simoncelli, N. C. Rust, Pinpointing the neural signatures of single-exposure visual recognition memory. *Proc Natl Acad Sci U S A* **118** (2021).
21. U. Rutishauser, I. B. Ross, A. N. Mamelak, E. M. Schuman, Human memory strength is predicted by theta-frequency phase-locking of single neurons. *Nature* **464**, 903-907 (2010).
22. M. Brown, J. Aggleton, Recognition memory: What are the roles of the perirhinal cortex and hippocampus? *Nature Reviews Neuroscience* **2**, 51-61 (2001).
23. M. T. Kucewicz *et al.*, High frequency oscillations are associated with cognitive processing in human recognition memory. *Brain* **137**, 2231-2244 (2014).
24. M. J. Ison, R. Quian Quiroga, I. Fried, Rapid Encoding of New Memories by Individual Neurons in the Human Brain. *Neuron* **87**, 220-230 (2015).
25. T. C. Sheehan, V. Sreekumar, S. K. Inati, K. A. Zaghloul, Signal Complexity of Human Intracranial EEG Tracks Successful Associative-Memory Formation across Individuals. *J Neurosci* **38**, 1744-1755 (2018).
26. S. Wirth *et al.*, Single neurons in the monkey hippocampus and learning of new associations. *Science* **300**, 1578-1581. (2003).
27. C. B. Kirwan, C. E. Stark, Medial temporal lobe activation during encoding and retrieval of novel face-name pairs. *Hippocampus* **14**, 919-930 (2004).
28. C. Ranganath, M. X. Cohen, C. Dam, M. D'Esposito, Inferior temporal, prefrontal, and hippocampal contributions to visual working memory maintenance and associative memory retrieval. *J Neurosci* **24**, 3917-3925 (2004).
29. K. Sakai, Y. Miyashita, Neural organization for the long-term memory of paired associates. *Nature* **354**, 152-155 (1991).
30. Y. D. Zhou, A. Ardestani, J. M. Fuster, Distributed and associative working memory. *Cereb Cortex* **17 Suppl 1**, i77-87 (2007).
31. U. Rutishauser, L. Reddy, F. Mormann, J. Sarnthein, The Architecture of Human Memory: Insights from Human Single-Neuron Recordings. *J Neurosci* **41**, 883-890 (2021).

32. A. Mayes, D. Montaldi, E. Migo, Associative memory and the medial temporal lobes. *Trends Cogn Sci* **11**, 126-135 (2007).
33. C. Van Petten, B. J. Luka, S. R. Rubin, J. P. Ryan, Frontal brain activity predicts individual performance in an associative memory exclusion test. *Cereb Cortex* **12**, 1180-1192 (2002).
34. O. Jensen, J. Kaiser, J. P. Lachaux, Human gamma-frequency oscillations associated with attention and memory. *Trends Neurosci* **30**, 317-324 (2007).
35. G. Buzsaki, C. A. Anastassiou, C. Koch, The origin of extracellular fields and currents - EEG, ECoG, LFP and spikes. *Nat Rev Neurosci* **13**, 407-420 (2012).
36. G. Kreiman *et al.*, Object selectivity of local field potentials and spikes in the inferior temporal cortex of macaque monkeys. *Neuron* **49**, 433-445 (2006).
37. R. Mukamel *et al.*, Coupling between neuronal firing, field potentials, and FMRI in human auditory cortex. *Science* **309**, 951-954 (2005).
38. P. Fries, J. Reynolds, A. Rorie, R. Desimone, Modulation of oscillatory neuronal synchronization by selective visual attention. *Science* **23**, 1560-1563 (2001).
39. M. R. Mercier *et al.*, Evaluation of cortical local field potential diffusion in stereotactic electro-encephalography recordings: A glimpse on white matter signal. *Neuroimage* **147**, 219-232 (2017).
40. G. McCarthy, A. C. Nobre, S. Bentin, D. D. Spencer, Language-related field potentials in the anterior-medial temporal lobe: I. Intracranial distribution and neural generators. *J Neurosci* **15**, 1080-1089 (1995).
41. A. Bansal *et al.*, Neural Dynamics Underlying Target Detection in the Human Brain. *Journal of Neuroscience* **34**, 3042-3055 (2014).
42. U. Mitzdorf, Current source-density method and application in cat cerebral cortex: investigation of evoked potentials and EEG phenomena. *Physiological Reviews* **65**, 37-99 (1985).
43. N. K. Logothetis, The neural basis of the blood-oxygen-level-dependent functional magnetic resonance imaging signal. *Philos Trans R Soc Lond B Biol Sci* **357**, 1003-1037 (2002).
44. R. O'Brien, A caution regarding rules of thumb for variance inflation factors. *Quality & Quantity: International Journal of Methodology* **41**, 673-690 (2007).
45. Y. Agam *et al.*, Robust selectivity to two-object images in human visual cortex. *Current Biology* **20**, 872-879 (2010).
46. E. Tulving, H. J. Markowitsch, F. E. Craik, R. Habib, S. Houle, Novelty and familiarity activations in PET studies of memory encoding and retrieval. *Cereb Cortex* **6**, 71-79 (1996).
47. Y. Jiang, J. V. Haxby, A. Martin, L. G. Ungerleider, R. Parasuraman, Complementary neural mechanisms for tracking items in human working memory. *Science* **287**, 643-646 (2000).
48. M. Lundqvist *et al.*, Gamma and Beta Bursts Underlie Working Memory. *Neuron* **90**, 152-164 (2016).
49. B. P. Staresina *et al.*, Recollection in the human hippocampal-entorhinal cell circuitry. *Nat Commun* **10**, 1503 (2019).
50. H. C. Bergmann, M. Rijpkema, G. Fernandez, R. P. Kessels, Distinct neural correlates of associative working memory and long-term memory encoding in the medial temporal lobe. *Neuroimage* **63**, 989-997 (2012).

51. R. Habib, A. R. McIntosh, M. A. Wheeler, E. Tulving, Memory encoding and hippocampally-based novelty/familiarity discrimination networks. *Neuropsychologia* **41**, 271-279 (2003).
52. T. E. Chow, J. Rissman, Neurocognitive mechanisms of real-world autobiographical memory retrieval: insights from studies using wearable camera technology. *Ann N Y Acad Sci* **1396**, 202-221 (2017).
53. M. C. Duff, T. Wszalek, D. Tranel, N. J. Cohen, Successful life outcome and management of real-world memory demands despite profound anterograde amnesia. *J Clin Exp Neuropsychol* **30**, 931-945 (2008).
54. D. M. Nielson, T. A. Smith, V. Sreekumar, S. Dennis, P. B. Sederberg, Human hippocampus represents space and time during retrieval of real-world memories. *Proc Natl Acad Sci U S A* **112**, 11078-11083 (2015).
55. P. Misra, A. Marconi, M. Peterson, G. Kreiman, Minimal memory for details in real life events. *Sci Rep* **8**, 16701 (2018).
56. H. Tang *et al.*, Predicting episodic memory formation for movie events. *Scientific Reports* **6**, 30175 (2016).
57. T. Lin *et al.* (2015) Microsoft COCO: Common Objects in Context. in *arxiv:1405.0312v3*.
58. D. Brainard, The Psychophysics Toolbox. *Spatial Vision* **10**, 433-436 (1997).
59. D. Pelli, The VideoToolbox software for visual psychophysics: transforming numbers into movies. *Spatial Vision* **10**, 437-442 (1997).
60. I. Fried, M. Cerf, U. Rutishauser, G. Kreiman, *Single neuron studies of the human brain. Probing cognition.* (MIT Press, Cambridge, MA, 2014).
61. D. M. Groppe *et al.*, iELVis: An open source MATLAB toolbox for localizing and visualizing human intracranial electrode data. *J Neurosci Methods* **281**, 40-48 (2017).
62. A. M. Dale, B. Fischl, M. I. Sereno, Cortical surface-based analysis. I. Segmentation and surface reconstruction. *Neuroimage* **9**, 179-194 (1999).
63. A. Joshi *et al.*, Unified framework for development, deployment and robust testing of neuroimaging algorithms. *Neuroinformatics* **9**, 69-84 (2011).
64. R. S. Desikan *et al.*, An automated labeling system for subdividing the human cerebral cortex on MRI scans into gyral based regions of interest. *Neuroimage* **31**, 968-980 (2006).
65. J. Wu *et al.*, Accurate nonlinear mapping between MNI volumetric and FreeSurfer surface coordinate systems. *Hum Brain Mapp* **39**, 3793-3808 (2018).
66. J. Wang, A. Tao, W. S. Anderson, J. R. Madsen, G. Kreiman, Mesoscopic physiological interactions in the human brain reveal small-world properties. *Cell Rep* **36**, 109585 (2021).
67. A. Bansal *et al.*, Temporal stability of visually selective responses in intracranial field potentials recorded from human occipital and temporal lobes. *Journal of Neurophysiology* **108**, 3073-3086 (2012).
68. P. Mitra, H. Bokil, *Observed brain dynamics* (Oxford University Press, New York 2008).
69. Y. Xiao *et al.*, Cross-task specificity and within-task invariance of cognitive control processes. *Cell Rep* **42**, 111919 (2023).
70. J. Nelder, R. Wedderburn, Generalized Linear Models. *Journal of the Royal Statistical Society. Series A (General)* **135**, 370-384 (1972).
71. T. Hastie, R. Tibshirani, *Generalized additive models* (Chapman and Hall/CRC, 1990).
72. C. F. Dormann *et al.*, Collinearity: a review of methods to deal with it and a simulation study evaluating their performance. *Ecography* **36**, 27-46 (2013).

73. R. E. Welsch, E. Kuh, Linear regression diagnostics. *National Bureau of Economic Research* (1977).
74. D. Gujarati, Use of Dummy Variables in Testing for Equality Between Sets of Coefficients in Linear Regressions: A Generalization. *The American Statistician* **24**, 18-22 (1970).

Figures and Tables

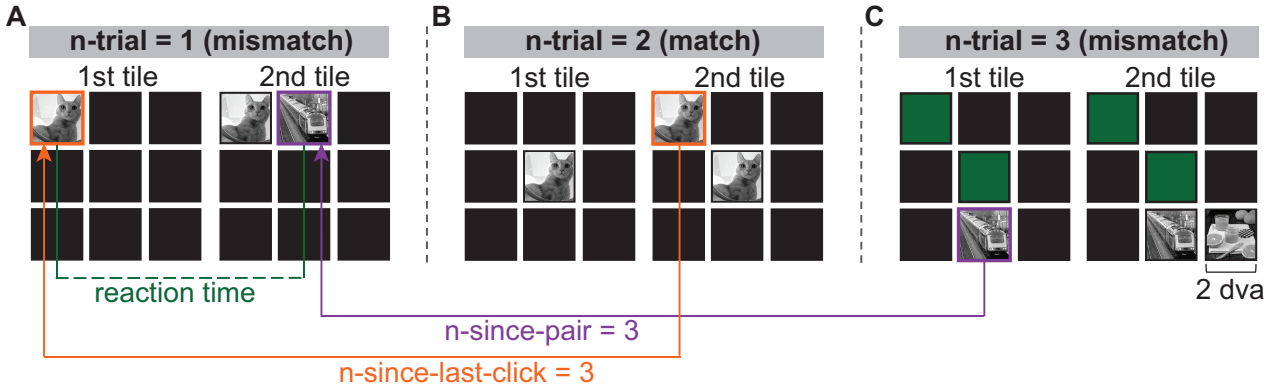

Figure 1. Experimental paradigm

A-C. Three consecutive trials in a 3×3 board. In each trial, two tiles were flipped sequentially in a self-paced manner (1st tile, then 2nd tile). If the two tiles contained different images (**A**, **C**, **mismatch**), both tiles reset to their original active (black) state after 1 second. If both tiles contained the same image (**B**, **match**), they turned green after 1 second and stayed green for the remainder of the block. Three behavioral predictors used in the generalized linear models (GLM) are defined here: reaction time (the time between the 1st and 2nd tile within a trial), n-since-last-click (the number of clicks elapsed since the same tile was clicked last), and n-since-pair (the number of clicks elapsed since the last time a given tile's matching pair was clicked). Each tile spanned approximately 2 degrees of visual angle (dva) in size. See also **Movie S1**.

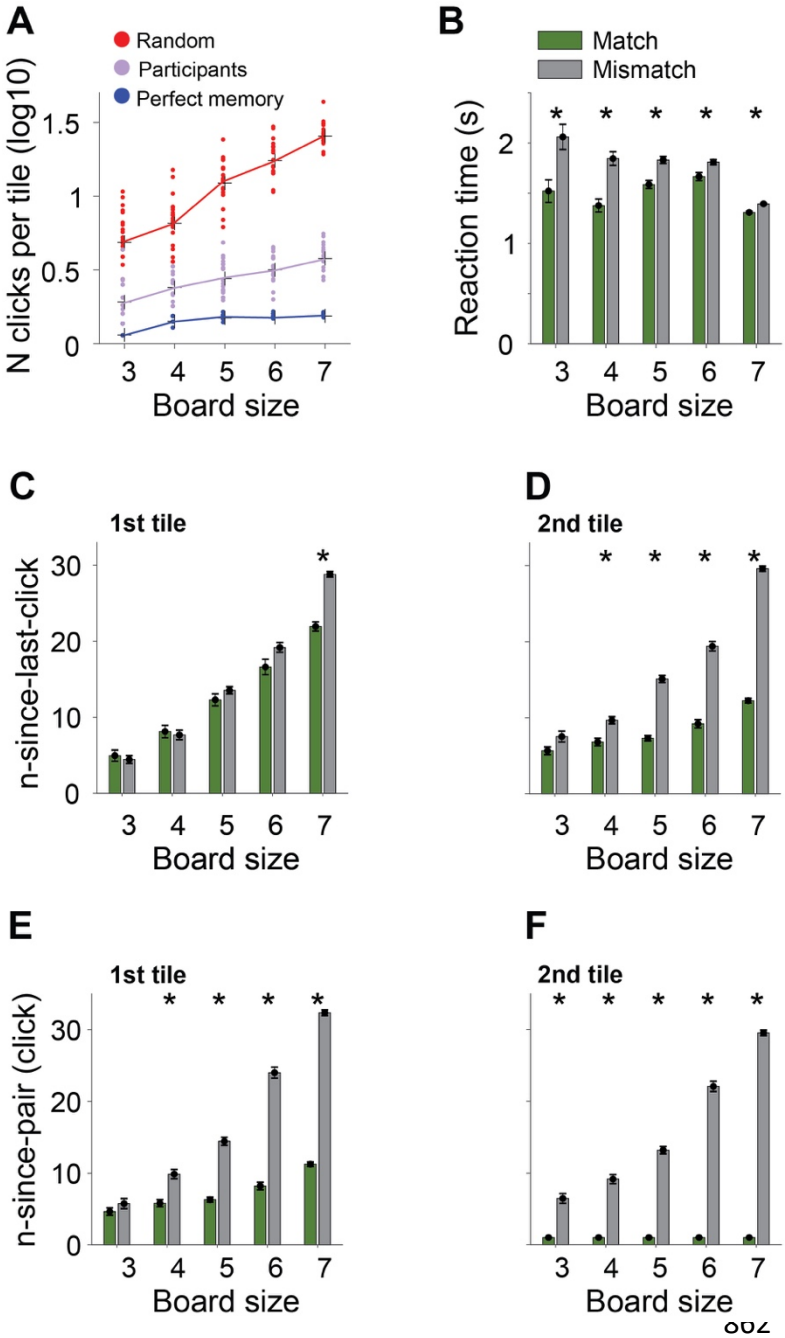

Figure 2. Behavioral measures show that participants thrived in the task and that finding matching pairs displayed classical memory effects

A. Number of clicks per tile (log scale) as a function of board size for random simulation model (red, n=20), perfect memory simulation model (blue, n=20), and epilepsy patient participants (purple, n=20) (**Methods**). Perfect memory simulation models may generate different number of clicks per tile because the click location for new tiles was randomized. The performance of epilepsy patients was better than the random model and worse than the perfect model. The number of clicks per tile increased as board size incremented. **B.** Reaction times for match (green) and mismatch (gray) trials for different board sizes. Asterisks denote significant difference between match and mismatch trials (permutation test, 5,000 iterations, α=0.01). Reaction time of mismatch trials was longer than match trials. **C-F.** Average n-since-last-click (**C**, **D**) and n-since-pair (**E**, **F**) for the 1st tile (**C**, **E**) and the 2nd tile (**D**, **F**) for each board size. Asterisks denote significant difference between match and mismatch trials (permutation test, 5,000 iterations, α=0.01). For n-since-last-click, trials in which a tile was clicked for the 1st time were excluded in this figure. For n-since-pair, trials in which any tile's matching pair had not been seen before were excluded in this figure. All error bars indicate s.e.m. (n=20 participants).

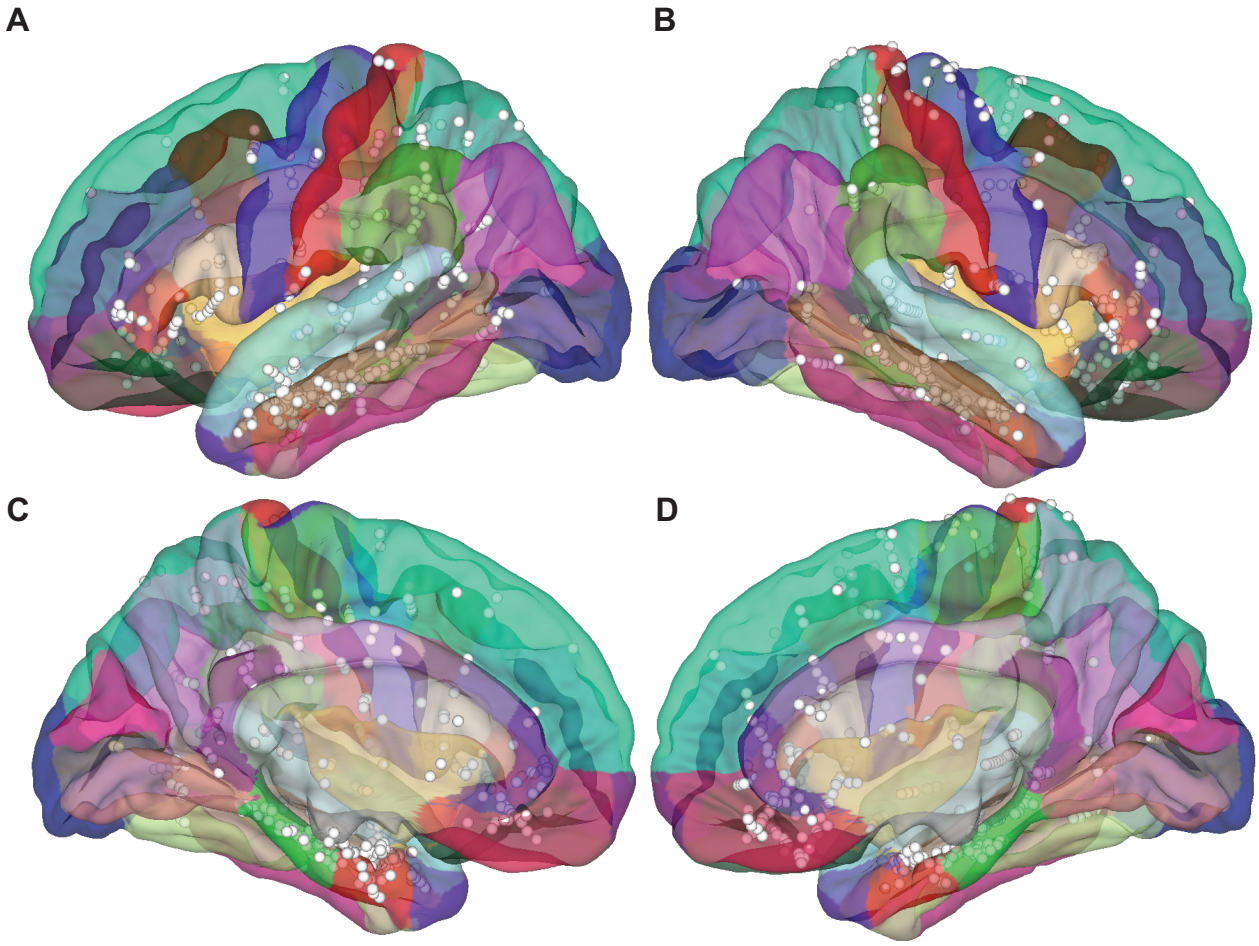

Figure 3. **Locations of electrodes in the gray matter**

Each circle shows a bipolarly referenced electrode (n=676), overlayed on the Desikan-Killiany Atlas with different views: **A**: left lateral; **B**: right lateral; **C**: left medial; **D**: right medial. The colors reflect the Desikan-Killiany parcellation (Desikan et al, 2006). Locations of white matter electrodes are reported in **Figure S2** (see also **Table S2**).

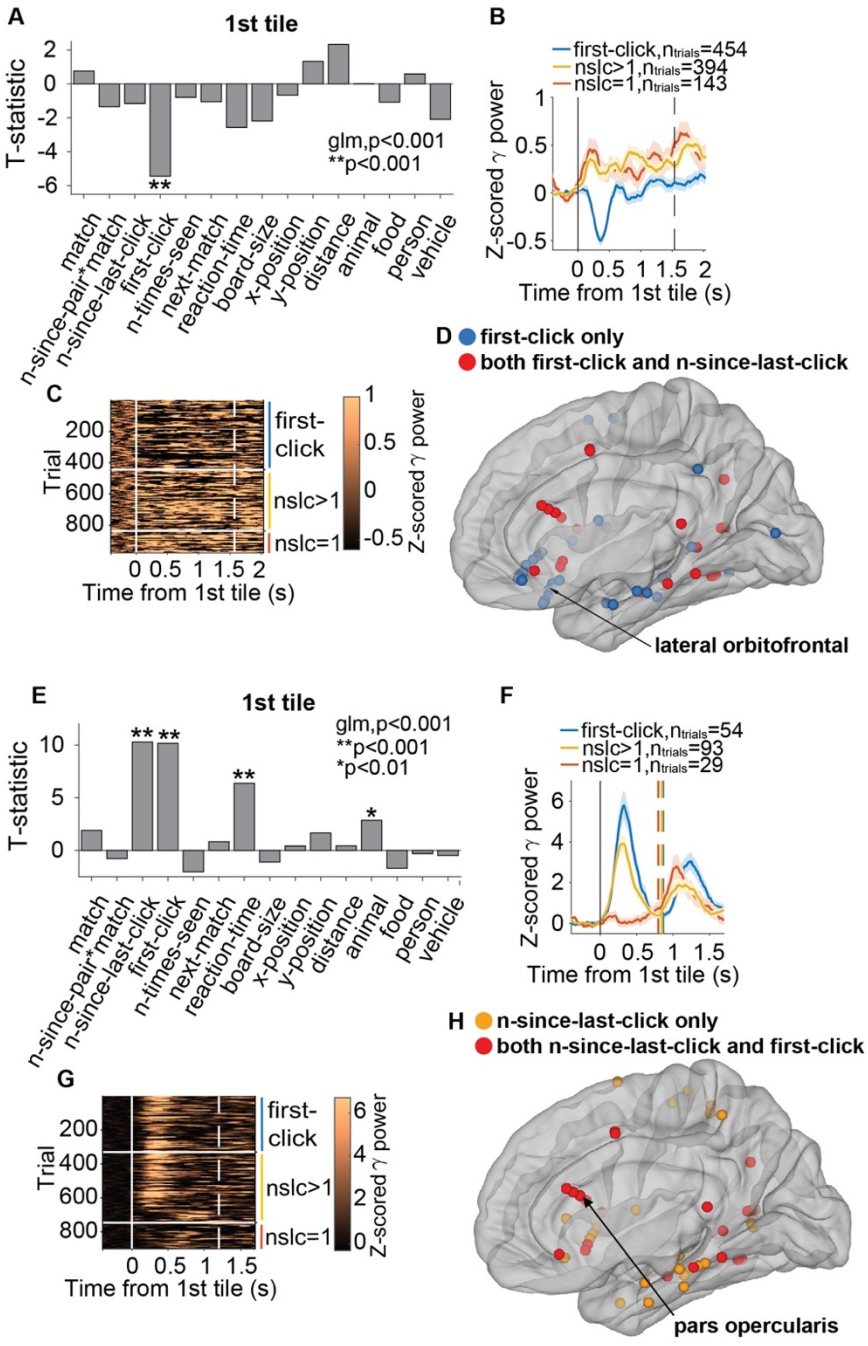

Figure 4. Neural signals reflect novelty and familiarity

Panels show two example electrodes, one in the right lateral orbitofrontal cortex (**A**-**D**), one in the left pars opercularis (**D**-**H**), and population locations in **D**, **H**.

A, **E**. T-statistic of each predictor in the GLM analyses (**Methods**). Asterisks indicate statistically significant predictors for the neural signals.

B, **F**. Z-scored gamma band power aligned to the 1st tile onset (solid vertical line) for novel tiles (blue), unfamiliar tiles (n-since-last-click>1, yellow), and familiar tiles (n-since-last-click=1, red). The vertical dashed line indicates the mean reaction time. Multiple dashed lines in **F** indicate reaction time equalization (**Methods**). The time axis extends from 400 ms before the click to 500 ms after the average reaction time. **F** displays only trials after RT equalization (**Methods**). Shaded error bars indicate s.e.m.

C, G. Raster plots showing the z-scored gamma power in individual trials ordered by first-click and then larger to smaller n-since-last-click; division indicated by white horizontal lines/spaces and colored vertical bars.

D. Locations of all electrodes where first-click was a significant predictor during the 1st tile. Blue: first-click only; red: both first-click and n-since-last-click were significant predictors.

H. Locations of all electrodes where n-since-last-click was a significant predictor during the 1st tile. Orange: n-since-last-click only; red: both n-since-last-click and first-click were significant predictors. All electrodes were reflected on one hemisphere for display purposes.

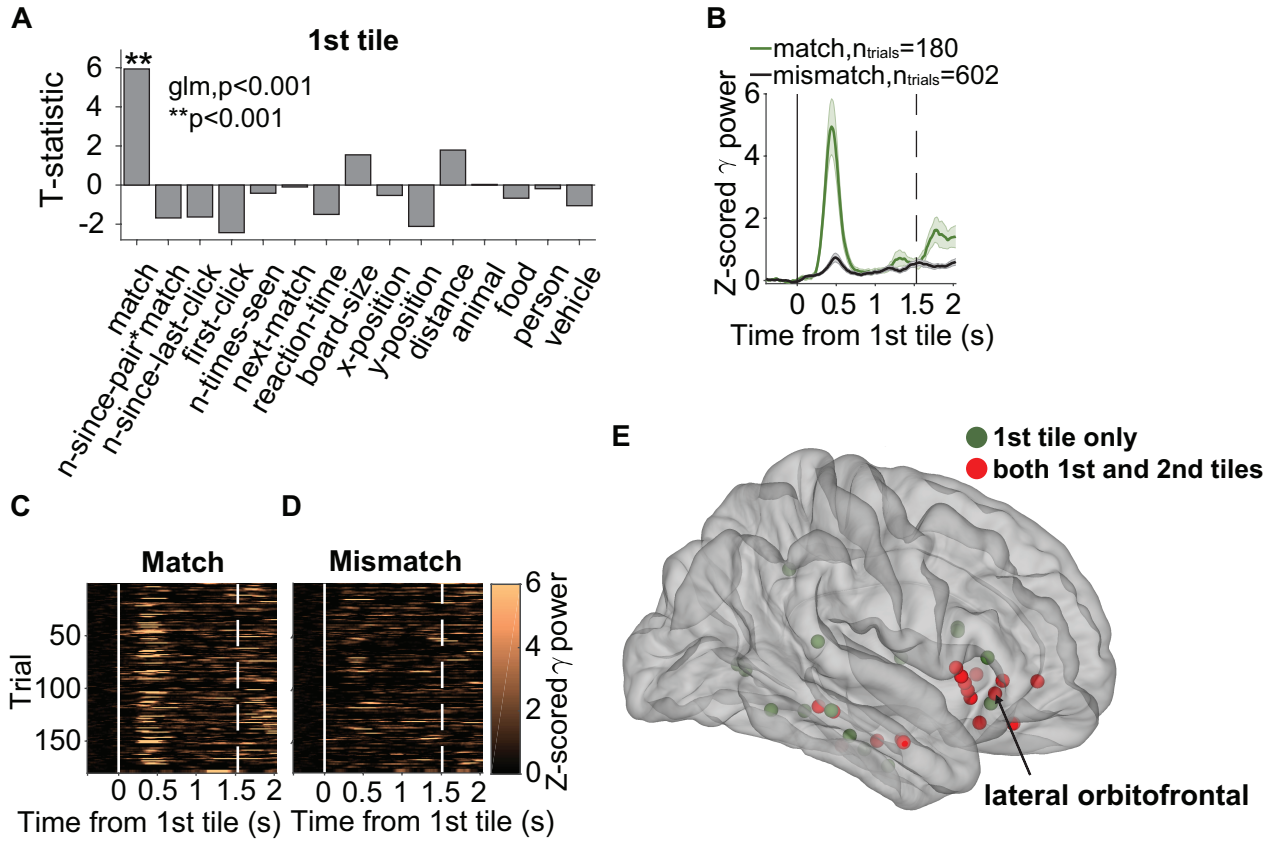

Figure 5. Neural signals predict correct retrieval

Panels show an example electrode in the right lateral orbitofrontal cortex (see arrow in part **E**) and population locations in **E**. The format follows **Figure 4**. **A.** T-statistic of each predictor in the GLM analysis. Asterisks indicate statistically significant predictors for the neural signals. **B**. Z-scored gamma band power aligned to the 1st tile onset (solid vertical line) for match trials (green) and mismatch trials (black). The vertical dashed line indicates the mean reaction time. Shaded error bars indicate s.e.m. **C**-**D**. Raster plots showing the gamma power in individual trials for match (left) and mismatch (right) trials. **E**. Locations of all electrodes where match was a significant predictor during the 1st tile only (green) and during both tiles (red). All electrodes were reflected on one hemisphere for display purposes.

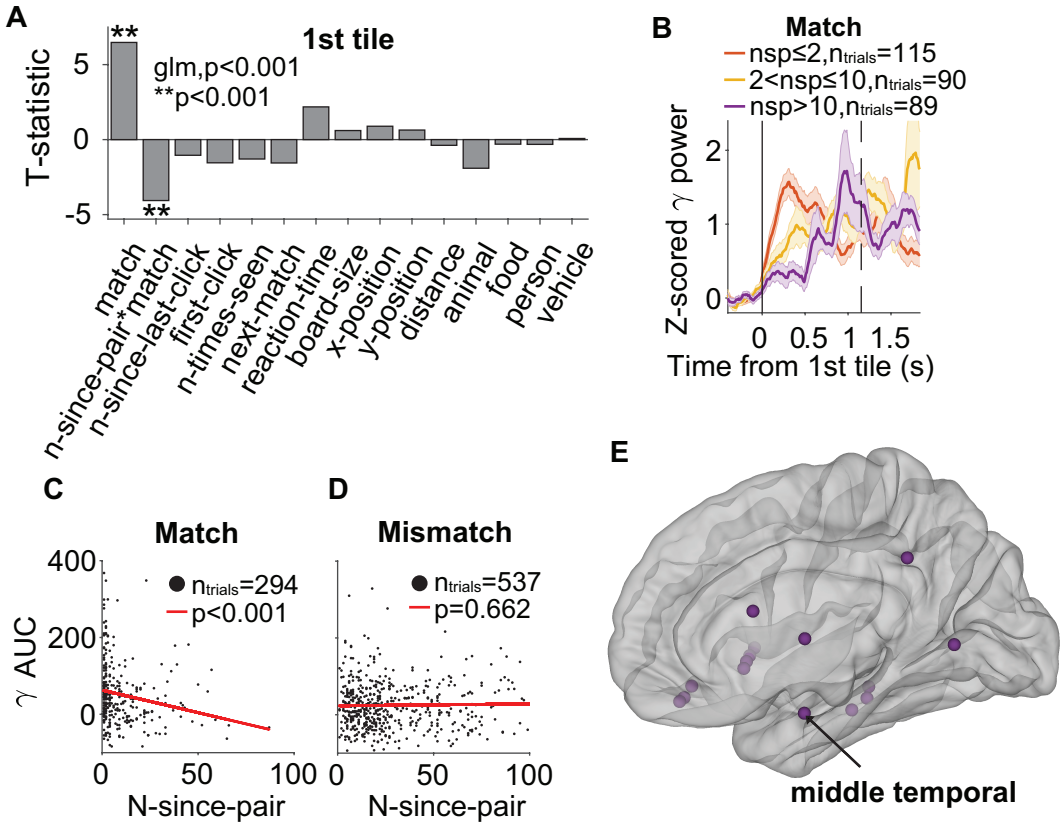

Figure 6. Neural signals reflect the strength of memory retrieval

Panels show an example electrode in the left middle temporal gyrus (see arrow in part **E**) and population locations in **E**. **A**. T-statistic of each predictor in the GLM analyses. Asterisks indicate significant predictors for the neural signals. **B**. Z-scored gamma band power aligned to the 1st file onset (solid vertical line) for match trials with small n-since-pair (nsp) (red, stronger memories), intermediate nsp (yellow), and large nsp (purple, weaker memories). The vertical dashed line indicates the mean reaction time. Shaded error bars indicate s.e.m. **C-D**. Scatter plots of the area under the curve (AUC) of the gamma band power as a function of nsp for match trials (**C**) and mismatch trials (**D**). Each dot represents one trial. Red lines show linear fits to the data. **E**. Locations of all electrodes where nsp was a significant predictor. All electrodes were reflected on one hemisphere for display purpose.

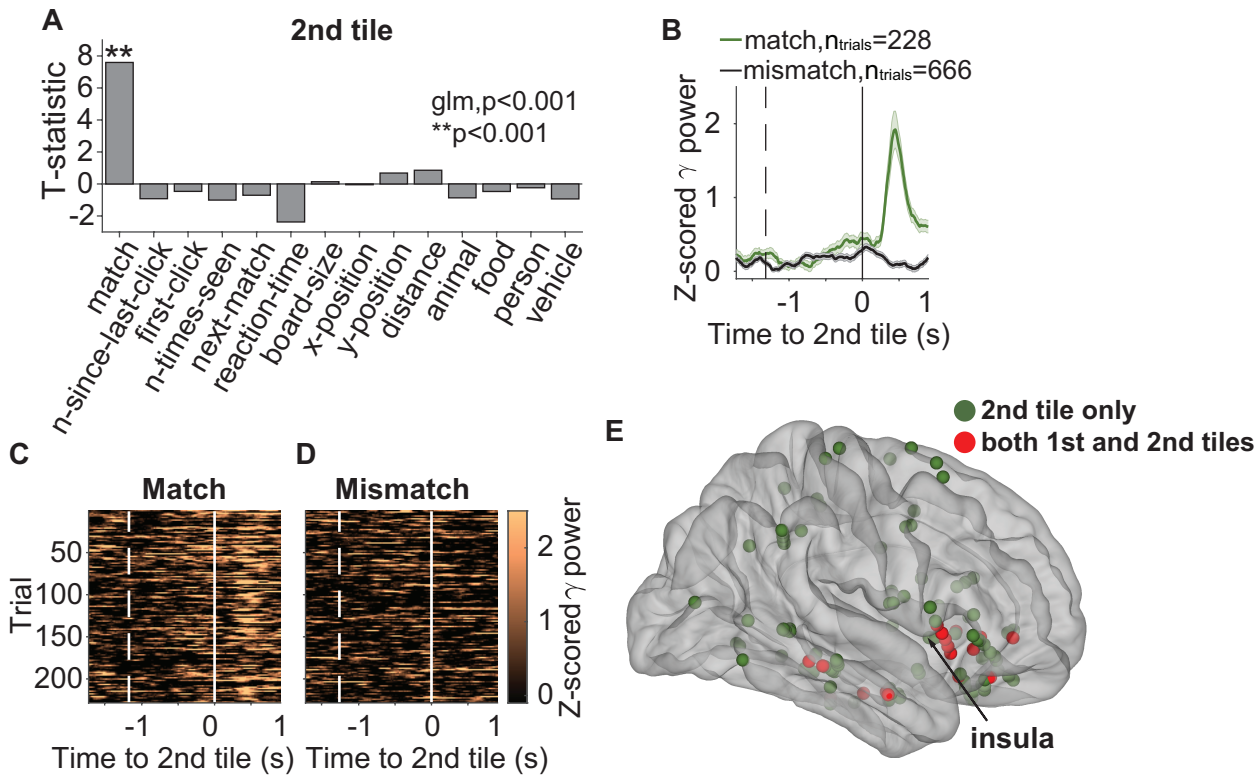

Figure 7. Neural signals after the second tile reflect correct retrieval

Panels show an example electrode located in the insula (see arrow in part **E**) and population locations. **A**. T-statistic of each predictor in the GLM analyses for the responses after the 2nd tile. Asterisks indicate significant predictors of neural signals. **B**. Z-scored gamma band power aligned to the onset of the 2nd tile (solid vertical line) for match (green) and mismatch (black) trials. The dashed line indicates the mean onset of the 1st tile. **C**-**D**. Raster plots showing the gamma band power in individual trials for match (left) and mismatch (right) trials. **E**. Locations of all electrodes where match was a significant predictor of neural responses after the 2nd tile only (green) or during both tiles (red). All electrodes were reflected on one hemisphere for display purpose.

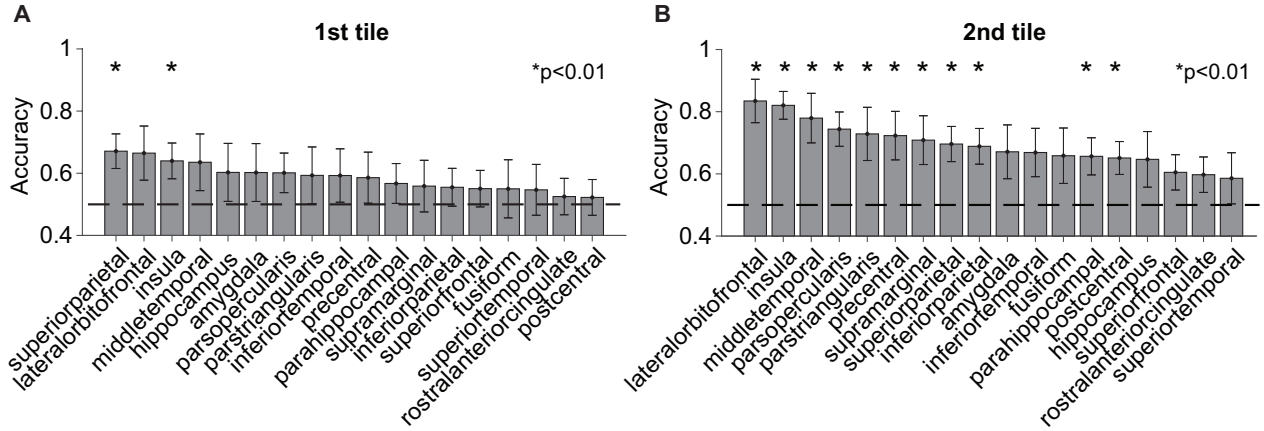

Figure 8. Machine learning decoding of match versus mismatch for all channels within each brain region

Average decoding accuracy for each brain region (**Methods**) using neural responses after the 1st tile (**A**) or after the 2nd tile (**B**). Brain regions are ordered from higher to lower average decoding accuracy. The dashed horizontal line indicates chance accuracy. Asterisks denote significant decoding accuracy above chance (α=0.01). All error bars indicate SD (n=1,000 iterations).

Tables

Predictor	Description	Which tile
match	Whether the trial was a match or mismatch	both
n-since-pair*match	how many clicks ago the tile's pair was clicked (matched trials only)	1st
n-since-last-click	how many clicks ago the same tile was clicked	both
first-click	Whether a tile was clicked the very first time	both
n-times-seen	number of times the same image had been previously clicked	both
next-match	whether the next trial was a match or mismatch	both
reaction-time	time between the 1st and 2nd tile	both
board-size	Total number of tiles in the current block	both
x-position	x position in pixel	both
y-position	y position in pixel	both
distance	distance between the 2nd tile of the current trial and the 1st tile of the next trial in pixel	both
animal	image belonged to animal category	both
food	image belonged to food category	both
person	image belonged to person category	both
vehicle	image belonged to vehicle category	both

Table 1. Predictors in the generalized linear models, their definitions, and applicable tiles.

Supplementary Materials

The Supplementary Material (separate file) includes:

1 supplementary movie

9 supplementary tables

12 supplementary figures

Figure S1

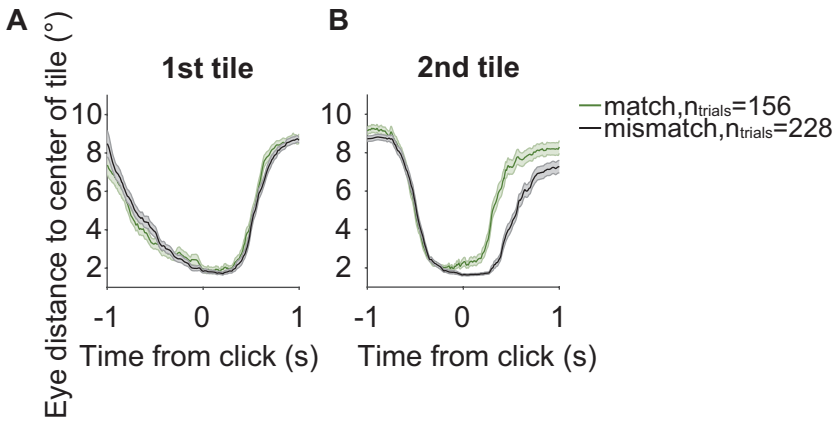

Figure S1. Participants' eye movements tracked the clicked locations.
Eye movements were similar during match and mismatch trials for the 1st tile, and for the 2nd tile before click time, but not for the 2nd tile after click time, when equalizing the reaction time and distances between the 1st and 2nd tiles. Line traces (mean±s.e.m) indicate the average distance in visual angle between gaze and the center of the tile clicked for match (green) and mismatch (black) trials. Reaction times (RT) and distances between the 1st and 2nd tiles were equalized (mean RT ± 200ms; mean distance ± 3°). **A**. No significant difference in eye-movements between match and mismatch was found during clicking the 1st tile. **B**. No significant difference in eye movements between match and mismatch was found before clicking the 2nd tile. Participants' gaze moved faster away from the 2nd tile in match trials than mismatch trials after the click: within the 1 second window after time zero, the distance from the gaze to the center of the tile was on average 1.76 dva (degrees of visual angle) larger for match than mismatch trials.

Figure S2

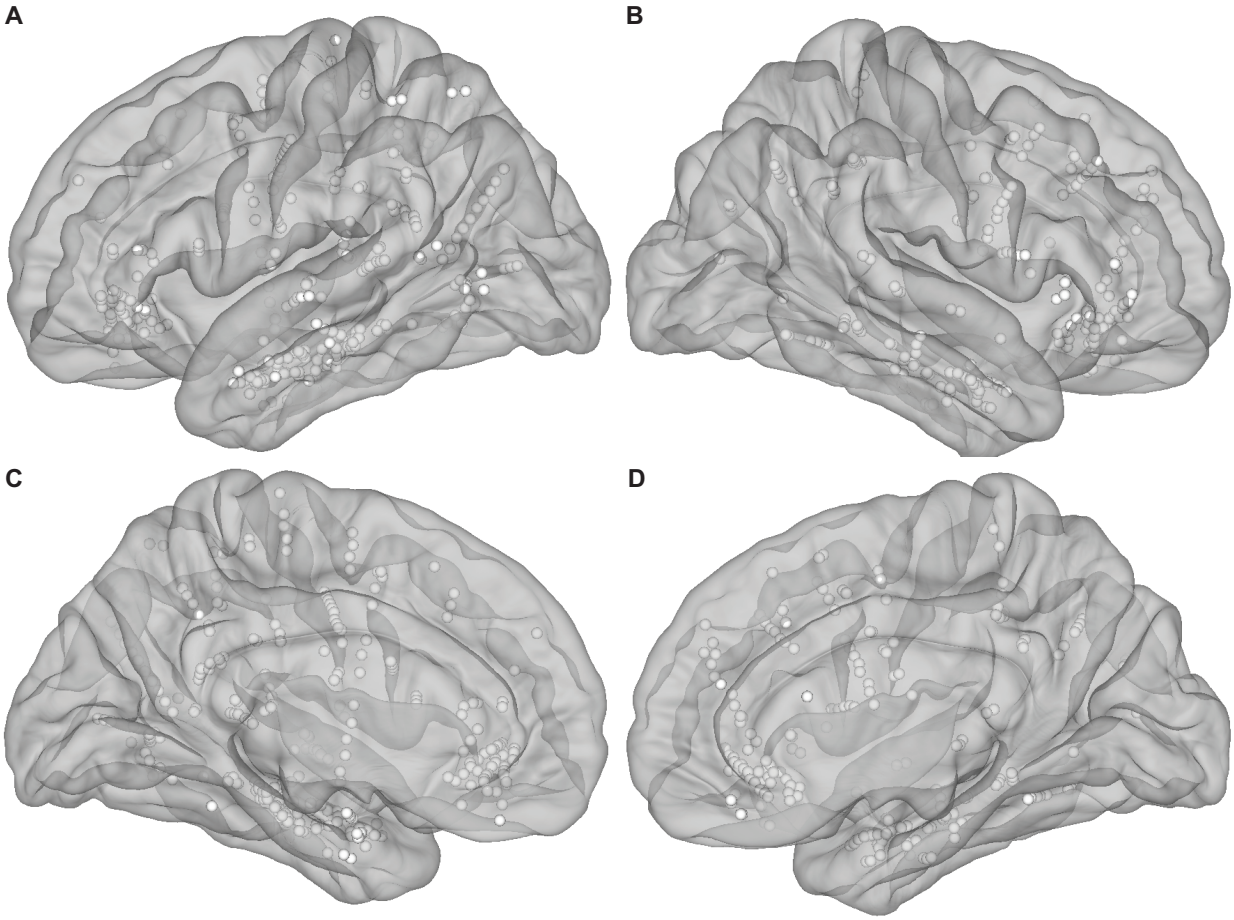

Figure S2. **Locations of all analyzed electrodes in the white matter.** Each sphere reflects one of each pair of nearby electrodes that were bipolarly referenced (n=492, **Table S2**). **A**: left lateral view; **B**: right lateral view; **C**: left medial view; **D**: right medial view. The location of gray matter electrodes is shown in **Figure 3**.

Figure S3

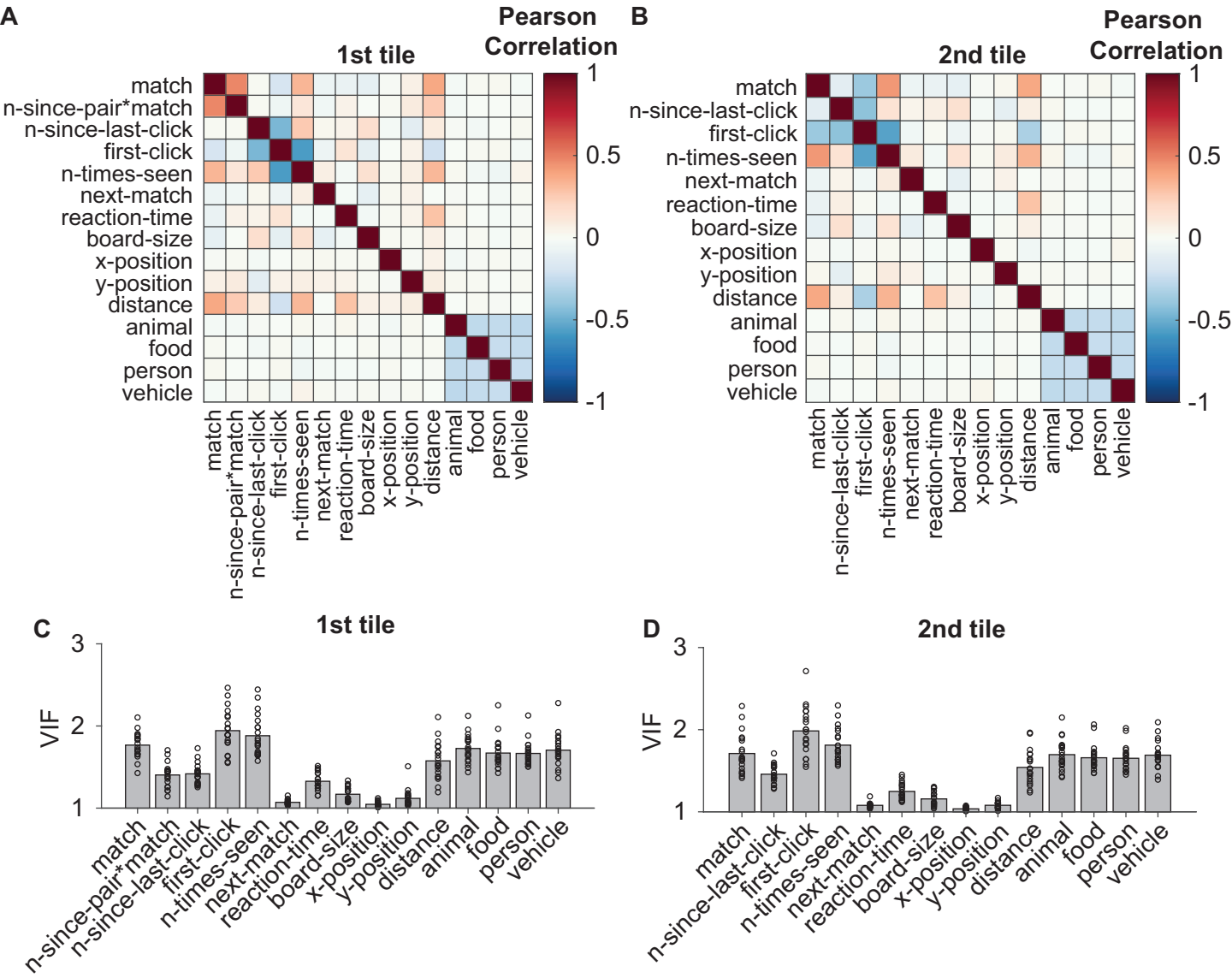

Figure S3. Correlation and collinearity among predictor variables.
A, **B**. Average across subjects of the Pearson correlation between pairs of predictors for the 1st tile (**A**) and the 2nd (**B**) tile. See color scale on the right. This is a symmetric matrix and the diagonal is 1, by definition. **Table 1** describes each of the predictors.
C, **D**. Variation Inflation Factor (VIF) (O'Brien, 2007) of each predictor for the 1st tile (**C**) and the 2nd (**D**) tile. Bar height indicates the average VIF of each predictor across all subjects. Dots represent the VIF of each predictor for each subject.

Figure S4

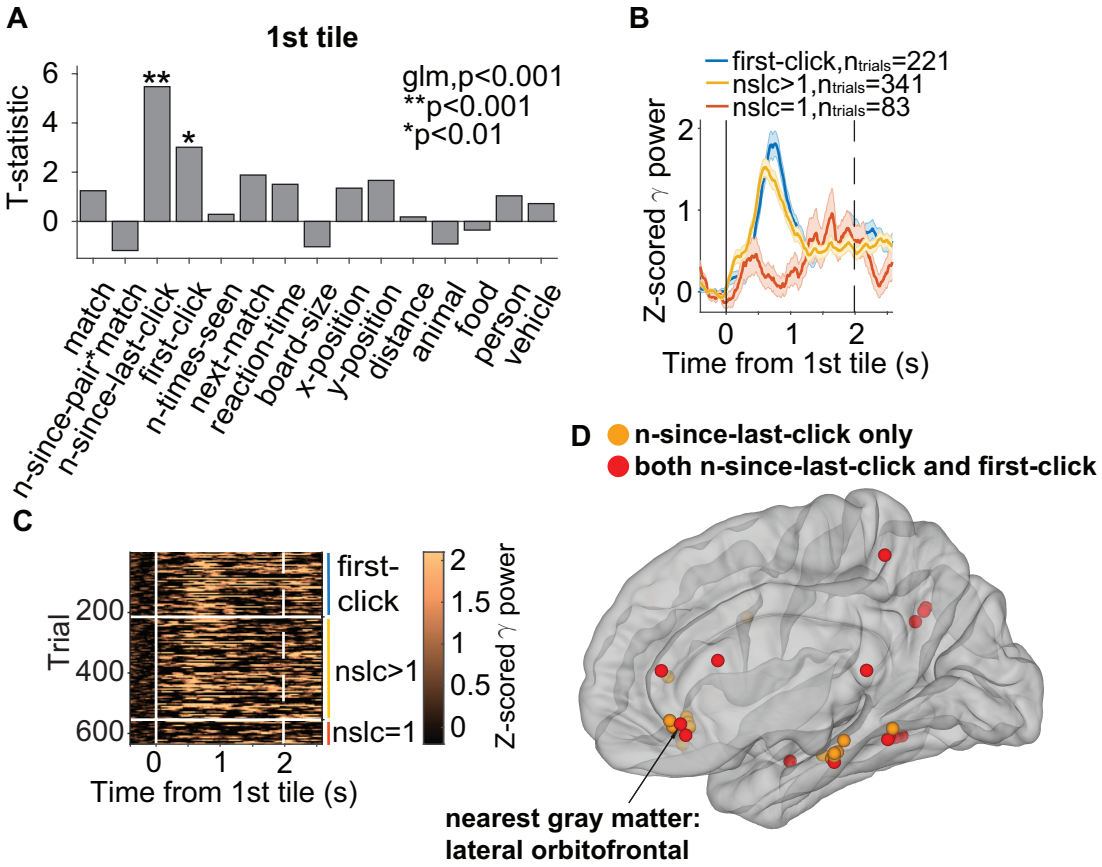

Figure S4. Neural signals in the white matter reflect novelty and familiarity

Panels show an example electrode in the white matter whose closest gray matter region is the left lateral orbitofrontal cortex (arrow in **D**). This figure follows the format of **Figure 4** in the main text.

A. T-statistic of each predictor in the GLM analysis (**Methods**). Asterisks indicate statistically significant predictors for the neural signals.

B. Z-scored gamma band power aligned to the 1st tile onset (solid vertical line) for novel tiles (blue), unfamiliar tiles (n-since-last-click>1, yellow), and more familiar tiles (n-since-last-click=1, red). The vertical dashed line indicates the mean reaction time. The time axis extends from 400 ms before the click to 500 ms after the average reaction time.

C. Raster plot showing the z-scored gamma power in individual trials ordered by first-click and then larger to smaller n-since-last-click; division indicated by white horizontal lines and colored vertical lines.

D. Locations of all white matter electrodes where n-since-last-click was a significant predictor during the 1st tile. Orange: n-since-last-click; red: both n-since-last-click and first-click were significant predictors. All electrodes were reflected on one hemisphere for display purposes.

Figure S5

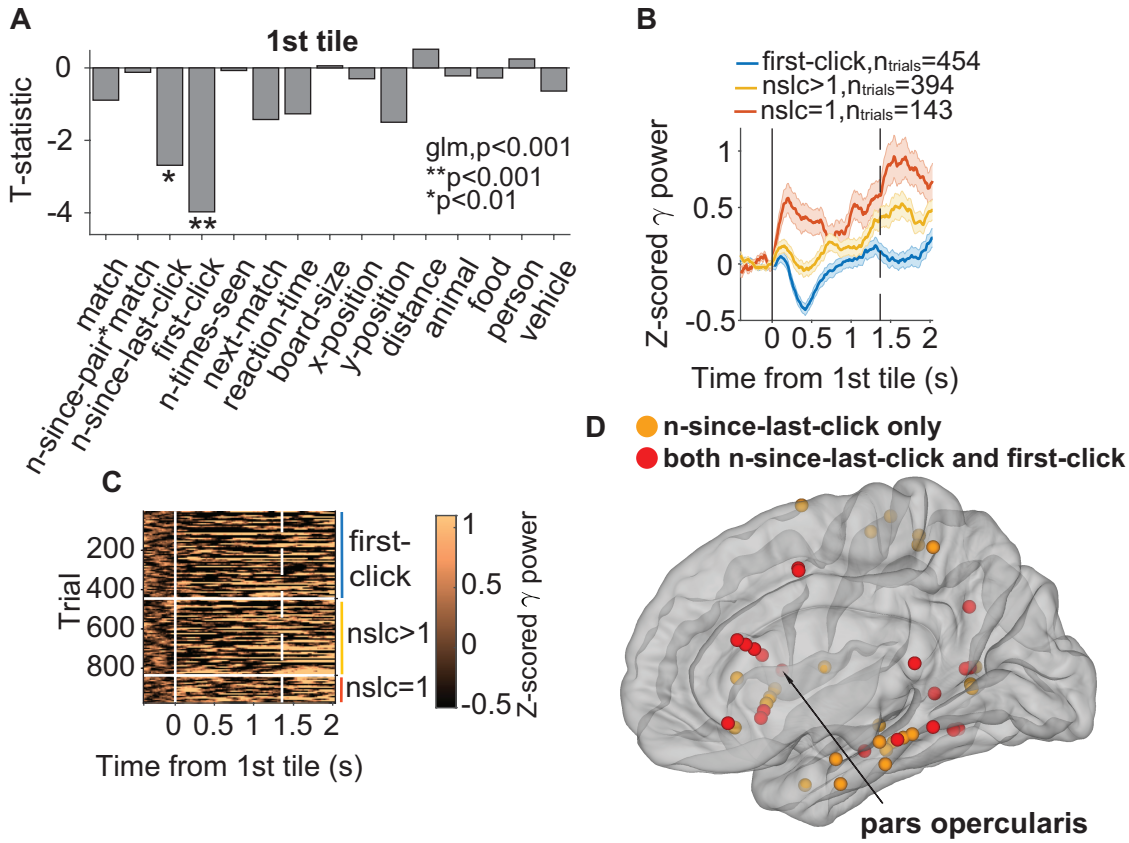

Figure S5. Neural signals reflect novelty and familiarity with a pattern different from that shown in Figure 4E-G.

This figure shows an example electrode in the right pars opercularis (gray matter, arrow in **D**), following the format of **Figure 4** in the main text. In contrast to **Figure 4E-G**, this electrode showed increased activity for more familiar trials.

A. T-statistic of each predictor in the GLM for the 1st tile. Asterisks indicate significant predictors for the gamma power AUC.

B. Z-scored gamma (30-150 Hz) power for first-click (blue), n-since-last-click>1 (yellow), and n-since-last-click=1 (red). Dashed line indicates the mean reaction time.

C. Raster plot showing the z-scored gamma power in individual trials ordered by first-click and then larger to smaller n-since-last-click; division indicated by white horizontal lines and colored vertical lines.

D. Locations of all n-since-last-click electrodes during the 1st tile. Orange: n-since-last-click only; red: both n-since-last-click and first-click were significant predictors. All electrodes were reflected on one hemisphere for display purposes.

Figure S6

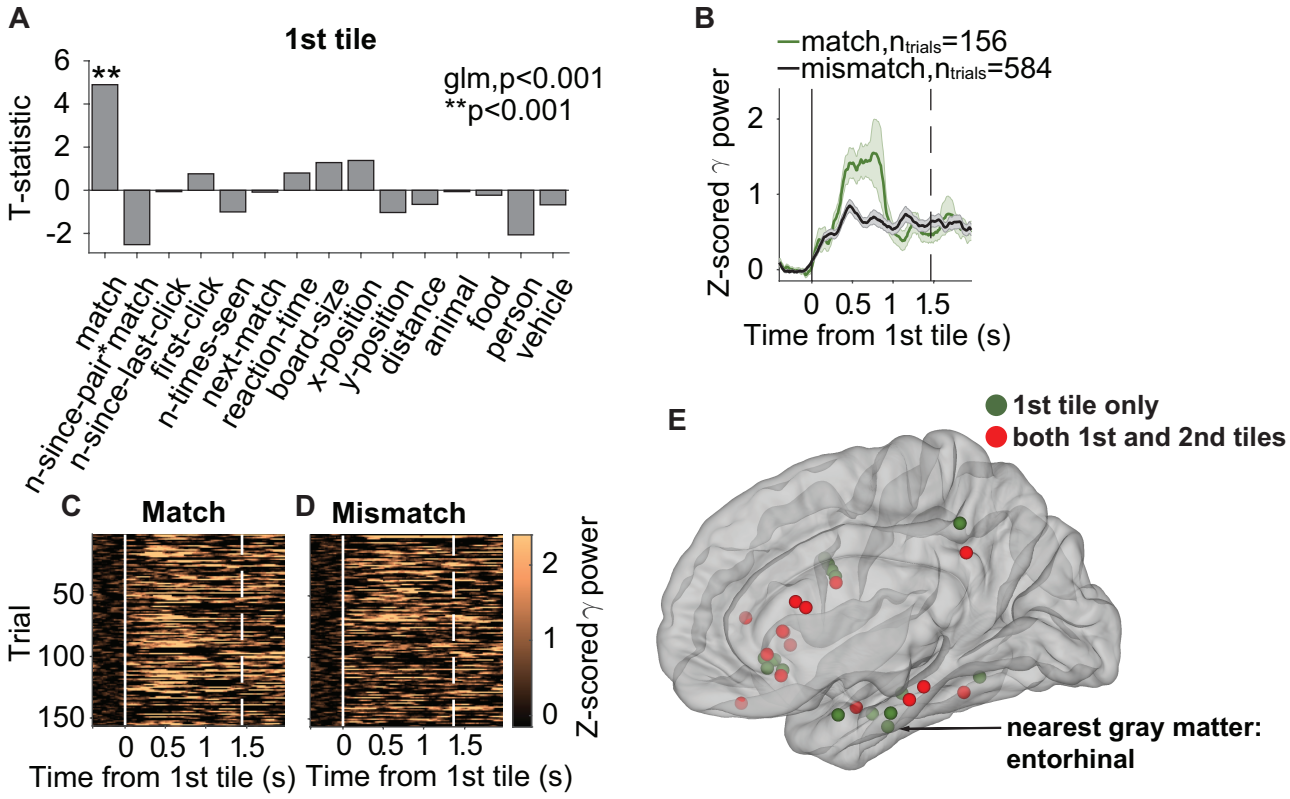

Figure S6. Neural signals in the white matter predict correct retrieval

Panels show an example electrode located in the white matter where the nearest gray matter region is the right entorhinal cortex (see arrow in **E**) as well as population locations in **E**. The format follows **Figure 4**.

A. t-statistic of each predictor in the GLM analysis. Asterisks indicate statistically significant predictors for the neural signals.

B. Z-scored gamma band power aligned to the 1st tile onset (solid vertical line) for match trials (green) and mismatch trials (black). The vertical dashed line indicates the mean reaction time. Shaded error bars indicate s.e.m.

C-D. Raster plots showing the gamma power in individual trials for match (**C**) and mismatch (**D**) trials.

E. Locations of all the white matter electrodes where match was a significant predictor during the 1st tile only (green) and during both tiles (red). All electrodes were reflected on one hemisphere for display purposes.

Figure S7

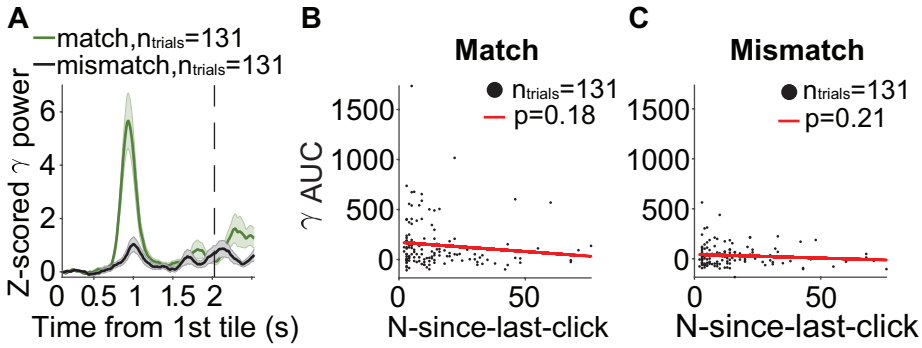

Figure S7. Match is the only predictor that accounts for the neural differences between match and mismatch

Panels shown the neural responses of an example electrode in the right lateral orbitofrontal cortex (same as in **Figure 5**) when equalizing the distribution of n-since-last click in match and mismatch trials.

A. Z-scored gamma (30-150 Hz) power during match (green) and mismatch (black) trials aligned to the 1st tile onset (solid line) after equalizing n-since-last-click values of match and mismatch trials by random subsampling. Dashed line indicates the mean reaction time.

B-C. Scatter plots of AUC of gamma power versus n-since-last-click for match (**B**) and mismatch (**C**) trials. Each dot represents data from one trial. Red lines represent linear fits of the data.

Figure S8

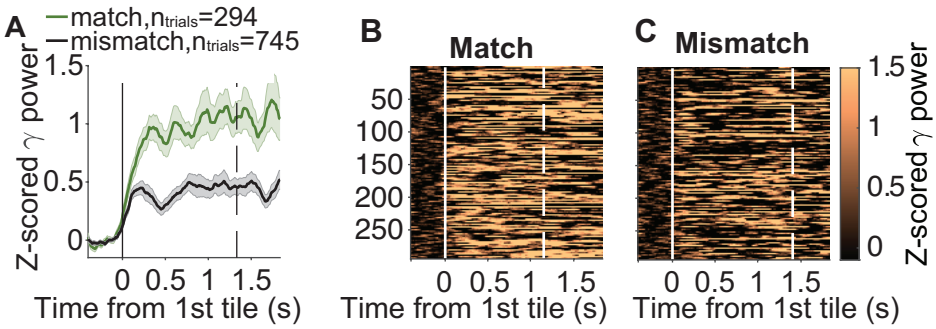

Figure S8. Neural signals predict correct retrieval with a pattern different from that shown in Figure 5

Panels show an example electrode located in the left middle temporal gyrus where "match" was a significant predictor for gamma activity.

A. Z-scored gamma (30-150 Hz) power during match (green) and mismatch (black) trials aligned to the 1st tile onset (solid line). Dashed line indicates the mean reaction time.

B-**C**. Raster plots showing the z-scored gamma power in individual match (**B**) and mismatch (**C**) trials. For display purposes, trial numbers of match and mismatch were equalized (**Methods**).

Figure S9

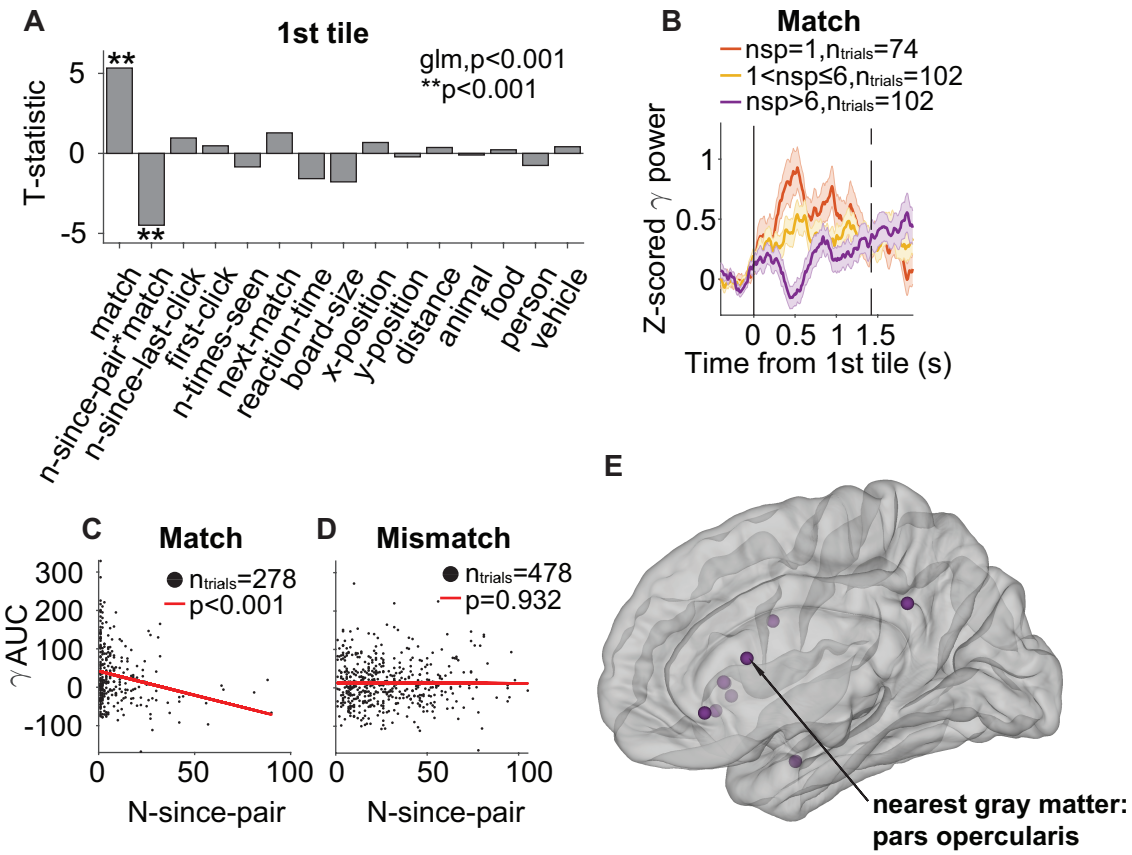

Figure S9. Neural signals in the white matter reflect the strength of memory retrieval
Panels show an example electrode in the white matter where the closest gray matter region is the left pars opercularis (see arrow in part **E**) and population locations in **E**.

A. T-statistic of each predictor in the GLM analysis. Asterisks indicate significant predictors for the neural signals.

B. Z-scored gamma band power aligned to the 1st tile onset (solid vertical line) for match trials with small n-since-pair (red, stronger memories), intermediate nsp (yellow), and large nsp (purple, weaker memories). The vertical dashed line indicates the mean reaction time. Shaded error bars indicate s.e.m.

C-D. Scatter plots of the area under the curve (AUC) of the gamma band power as a function of nsp for match trials (**C**) and mismatch trials (**D**). Each dot represents one trial. Red lines show linear fits to the data.

E. Locations of all white matter electrodes where nsp was a significant predictor. All electrodes were reflected on one hemisphere for display purposes.

Figure S10

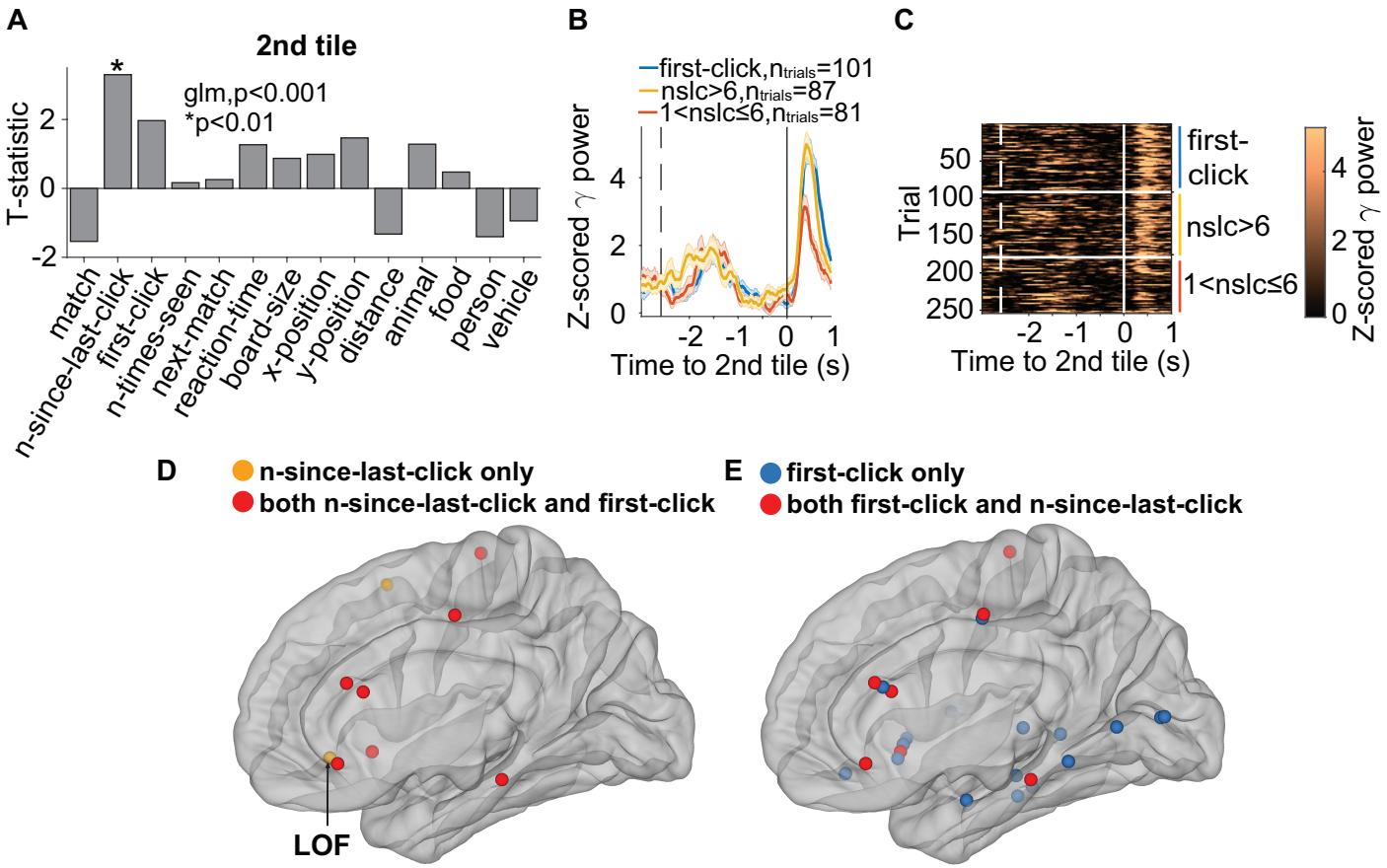

Figure S10. Neural signals after the second tile reflect familiarity and novelty
Panels show an example electrode in the right lateral orbitofrontal (LOF) cortex and population locations in **D**-**E**.

A. T-statistic of each predictor in the GLM analysis (**Methods**). Asterisks indicate statistically significant predictors for the neural signals.

B. Z-scored gamma band power aligned to the 2nd tile onset (solid vertical line) for novel tiles (blue), unfamiliar tiles (n-since-last-click>6, yellow), and familiar tiles (n-since-last-click≤1, red). The vertical dashed line indicates the mean onset of the 1st tile. The time axis extends from 400 ms plus the average reaction time before the click to 1,000 ms after the click.

C. Raster plots showing the z-scored gamma power in individual trials ordered by first-click and then larger to smaller n-since-last-click; division indicated by white horizontal lines/spaces and colored vertical bars.

D. Locations of all electrodes where n-since-last-click was a significant predictor during the 2nd tile. Orange: n-since-last-click only; red: both n-since-last-click and first-click were significant predictors.

E. Locations of all electrodes where first-click was a significant predictor during the 2nd tile. Blue: first-click only; red: both first-click and n-since-last-click were significant predictors. All electrodes were reflected on one hemisphere for display purposes.

Figure S11

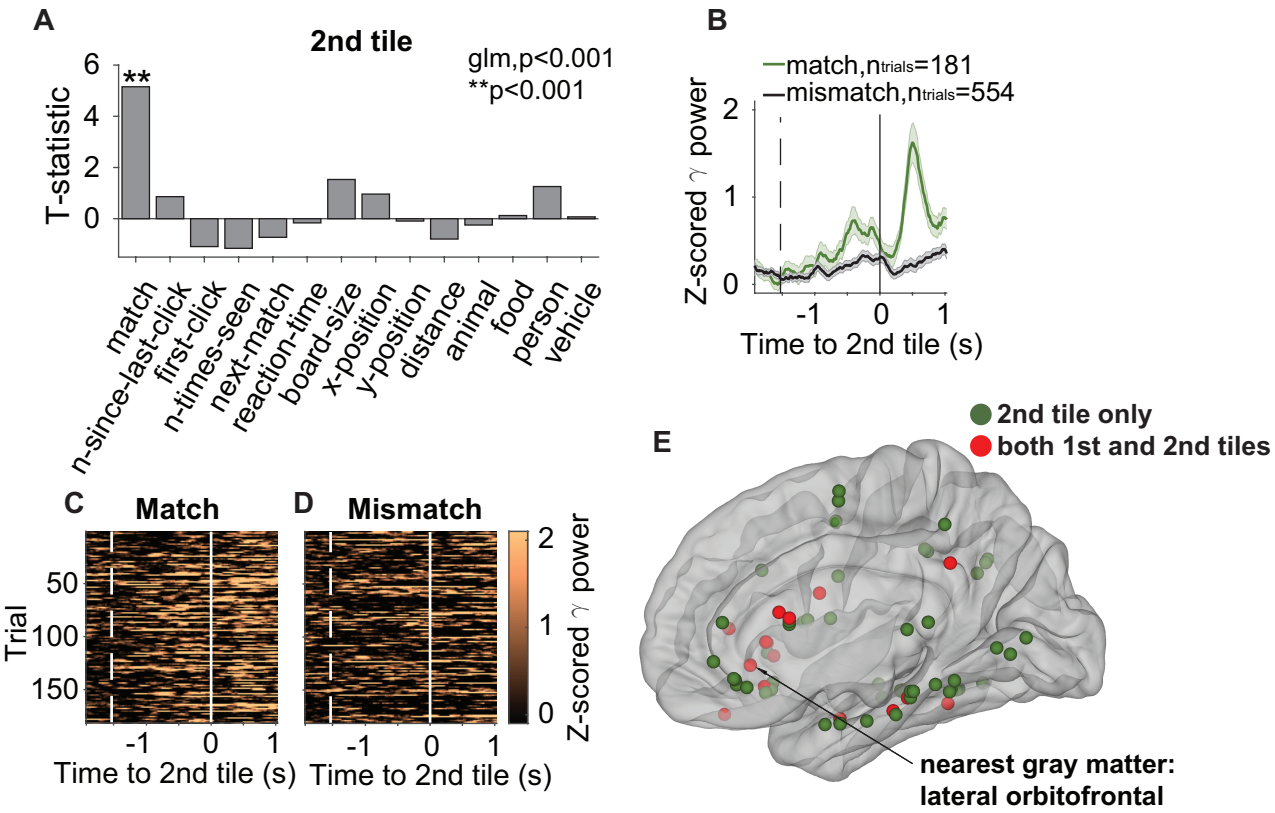

Figure S11. Neural signals in the white matter after the second tile reflect correct retrieval

Panels show an example electrode located in the white matter whose closest gray matter region is the right LOF (see arrow in part **E**).

A. T-statistic of each predictor in the GLM analysis for the responses after the 2nd tile. Asterisks indicate statistically significant predictors of neural signals.

B. Z-scored gamma band power aligned to the onset of the 2nd tile (solid vertical line) for match (green) and mismatch (black) trials. The dashed line indicates the mean onset of the 1st tile.

C-D. Raster plots showing the gamma band power in individual trials for match (left) and mismatch (right) trials.

E. Locations of all the white matter electrodes where match was a significant predictor during the 2nd tile only (green) and during both tiles (red). All electrodes were reflected on one hemisphere for display purposes.

Figure S12

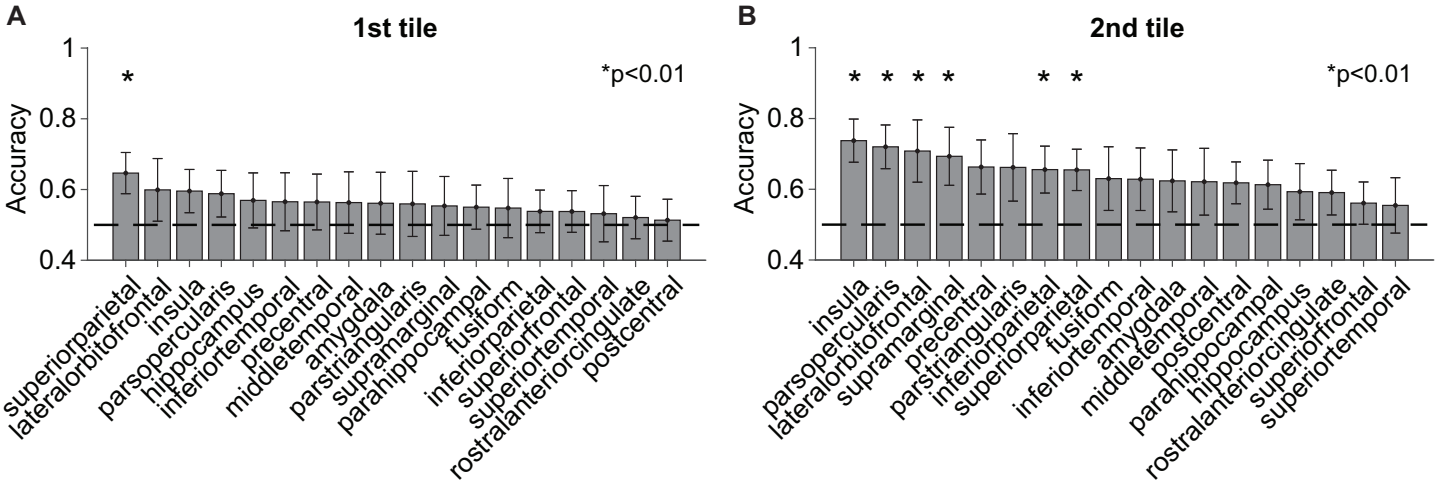

Figure S12. Decoding of match versus mismatch with random subsampling of 12 channels in each brain region.

Average decoding accuracy of each brain region (**Methods**) using neural responses after the 1st tile (**A**) and the 2nd tile (**B)**. The format follows **Figure 8**. Brain regions are ordered from higher to lower average decoding accuracy. Dashed horizontal lines indicate chance accuracy. Asterisks denote significant decoding accuracy above chance (α=0.01). All error bars indicate SD (n=1,000 iterations).

Table 1. Predictors in the generalized linear models, their definitions, and applicable tiles.

Predictor	Description	Which tile
match	Whether the trial was a match or mismatch	both
n-since-pair*match	how many clicks ago the tile's pair was clicked (matched trials only)	1st
n-since-last-click	how many clicks ago the same tile was clicked	both
first-click	Whether a tile was clicked the very first time	both
n-times-seen	number of times the same image had been previously clicked	both
next-match	whether the next trial was a match or mismatch	both
reaction-time	time between the 1st and 2nd tile	both
board-size	Total number of tiles in the current block	both
x-position	x position in pixel	both
y-position	y position in pixel	both
distance	distance between the 2nd tile of the current trial and the 1st tile of the next trial in pixel	both
animal	image belonged to animal category	both
food	image belonged to food category	both
person	image belonged to person category	both
vehicle	image belonged to vehicle category	both

Table S1: Information about each participant: hospital where data were recorded, gender, age, total number of electrodes implanted, number of electrodes analyzed in the gray matter, and number of electrodes analyzed in the white matter. All participants were right-handed.

Subject No.	Hospital	Gender	Age	# electrodes	# gray matter electrodes analyzed	# white matter electrodes analyzed
1	Xuanwu	female	22	85	37	21
2	Xuanwu	male	32	53	21	11
3	Xuanwu	male	19	114	32	68
4	Xuanwu	male	33	61	22	21
5	Xuanwu	male	35	71	28	27
6	Xuanwu	male	21	83	34	28
7	Xuanwu	male	26	86	34	35
8	Xuanwu	male	23	78	23	15
9	Xuanwu	female	47	34	11	4
10	Xuanwu	female	21	61	35	12
11	Xuanwu	female	26	78	17	9
12	BWH	female	32	51	29	0
13	BWH	female	31	74	24	19
14	BWH	female	26	60	15	15
15	BWH	male	22	104	30	21
16	BWH	female	52	98	35	28
17	BWH	male	44	58	20	9
18	BCH	male	18	154	85	26
19	BCH	female	12	188	97	46
20	BCH	male	15	159	47	77

Table S2: Distribution of electrode locations per hemisphere and brain region for the gray matter (left) and white matter (right). The location of any white matter electrode was based on its nearest gray matter region.

Gray matter				White matter (closest gray matter)			
Region	**Left**	**Right**	**Total**	**Region**	**Left**	**Right**	**Total**
amygdala	21	24	45	amygdala	0	0	0
bankssts	0	7	7	bankssts	5	2	7
caudalanteriorcingulate	1	3	4	caudalanteriorcingulate	1	0	1
caudalmiddlefrontal	1	5	6	caudalmiddlefrontal	1	7	8
entorhinal	5	0	5	cuneus	1	1	2
fusiform	15	10	25	entorhinal	2	2	4
hippocampus	36	31	67	fusiform	21	14	35
inferiorparietal	11	8	19	inferiorparietal	7	3	10
inferiortemporal	14	9	23	inferiortemporal	31	16	47
insula	13	15	28	insula	11	12	23
isthmuscingulate	6	0	6	isthmuscingulate	1	0	1
lateraloccipital	3	2	5	lateraloccipital	2	3	5
lateralorbitofrontal	19	32	51	lateralorbitofrontal	23	30	53
lingual	3	2	5	lingual	2	2	4
medialorbitofrontal	4	7	11	medialorbitofrontal	6	8	14
middletemporal	53	38	91	middletemporal	31	21	52
paracentral	4	0	4	paracentral	3	3	6
parahippocampal	10	13	23	parahippocampal	6	5	11
parsopercularis	11	5	16	parsopercularis	5	3	8
parsorbitalis	2	3	5	parsorbitalis	4	7	11
parstriangularis	13	19	32	parstriangularis	10	10	20
pericalcarine	0	1	1	pericalcarine	4	0	4
postcentral	8	12	20	postcentral	6	0	6
posteriorcingulate	4	3	7	posteriorcingulate	10	1	11
precentral	8	21	29	precentral	11	15	26
precuneus	3	0	3	precuneus	12	3	15
rostralanteriorcingulate	7	7	14	rostralanteriorcingulate	3	3	6
rostralmiddlefrontal	1	4	5	rostralmiddlefrontal	2	7	9
superiorfrontal	13	19	32	superiorfrontal	10	18	28
superiorparietal	8	12	20	superiorparietal	10	7	17
superiortemporal	26	21	47	superiortemporal	21	13	34
supramarginal	10	4	14	supramarginal	4	4	8
transversetemporal	6	0	6	transversetemporal	6	0	6
Total	**339**	**337**	**676**	**Total**	**272**	**220**	**492**

Table S3A. First tile GLM analysis for all gray matter electrodes that showed first-click as a significant predictor. Each column (starting from column 4) shows a separate predictor. Yellow rows indicate the example electrodes in **Figure 4** (first and second rows) and **Figure S4** (third row)**.** *: $p<0.01$. **: $p<0.001$. X: most significant predictor.

Region	Sub	Channel	match	n-since-pair* match	n-since-last-click	first-click	n-times-seen	next-match	RT	board-size	x-position	y-position	distance	animal	food	person	vehicle
Amygdala	7	3				* X											
Amygdala	15	81				*										** X	
bankssts	18	131				** X											
caudalmiddlefrontal	12	43				** X											
fusiform	1	42				*				*							** X
fusiform	3	11			*	*			**					** X			
fusiform	6	11			** X	*											*
fusiform	8	63			**	** X											
fusiform	16	92				* X											
inferiorparietal	3	71			** X	**			**							*	
inferiorparietal	18	150			** X	**				**		*					
inferiorparietal	18	151			** X	**					*					*	
inferiortemporal	18	143	*		**	** X											
inferiortemporal	18	144			** X	*											
insula	3	50				* X											
lateraloccipital	20	5				**			** X		*			*		*	
lateralorbitofrontal	3	40				** X			**	*			*				
lateralorbitofrontal	14	32				* X	*										
lateralorbitofrontal	15	22			** X	**		*	*			*					
lateralorbitofrontal	18	5				**				** X							
lateralorbitofrontal	18	6		*		** X				**							
lateralorbitofrontal	18	7				** X				*							
lateralorbitofrontal	18	20				** X	*										
lateralorbitofrontal	18	21				** X											
lateralorbitofrontal	18	22				** X											
lateralorbitofrontal	18	25	*		*	* X				*							
lateralorbitofrontal	18	26	**	**	**	** X				*							
lateralorbitofrontal	19	41				* X											
medialorbitofrontal	18	18				* X				*							
medialorbitofrontal	18	19				** X											
middletemporal	18	108				** X											
middletemporal	18	110	** X	*		*										*	
middletemporal	18	134			*	* X											
middletemporal	18	148				** X											
parahippocampal	9	27				* X											
parsopercularis	8	22			** X	**			**					*			
parsopercularis	8	23			**	** X			**							**	
parsopercularis	11	78			*	** X		*						*			*
parsopercularis	18	30				** X											
parsopercularis	18	32			*	** X											
parstriangularis	18	11				*				*				* X		*	
parstriangularis	18	13				**							** X				
parstriangularis	18	14				** X							*				
precentral	15	15			*	** X			**								
precentral	15	16			**	** X				**							
precentral	18	38				** X											
precentral	12	42				** X											
rostralmiddlefrontal	8	24			**	** X			**							*	
superiortemporal	2	44			*	** X											
supramarginal	2	32	** X	**		*	**		**				*				

Table S3B. First tile GLM analysis for all white matter electrodes that showed first-click as a significant predictor. Each column (starting from column 4) shows a separate predictor. Yellow row indicates the example electrode in **Figure S4**. *: p<0.01. **: p<0.001. X: most significant predictor.

Region	Sub	Channel	match	n-since-pair* match	n-since-last-click	first-click	n-times-seen	next-match	RT	board-size	x-position	y-position	distance	animal	food	person	vehicle
caudalanteriorcingulate	8	21	**		** X	**			**								
fusiform	3	28			** X	**			**				*			**	
fusiform	18	106				* X											
fusiform	18	138			**	** X				**	**					*	
fusiform	18	139			**	** X				*	*						
fusiform	18	140			**	** X			**	**	*						
fusiform	18	141			**	** X				*							
fusiform	18	142	*		**	** X				*							
inferiortemporal	1	43				*											** X
inferiortemporal	1	69				* X		*									
inferiortemporal	1	82				** X		*									
inferiortemporal	6	58				** X	**										
inferiortemporal	7	39			**	*			** X		*						
inferiortemporal	18	107				** X											
lateralorbitofrontal	15	21			** X	**			*								
lateralorbitofrontal	15	23			** X	*											
lateralorbitofrontal	18	4				** X											
lateralorbitofrontal	18	10				** X											
lateralorbitofrontal	18	23				** X											
lateralorbitofrontal	18	24				** X											
parahippocampal	1	10				*			*					** X	**	**	*
parsopercularis	18	31				** X		*									
parstriangularis	16	8				** X							*				
rostralmiddlefrontal	3	80				** X											
rostralmiddlefrontal	15	3			** X	**											
superiorfrontal	15	10				*			** X								
superiorparietal	3	20	*			*				* X							
superiorparietal	3	23			** X	**			*								
superiorparietal	3	70			** X	**											
superiorparietal	3	72			** X	**			*								
superiorparietal	3	73			** X	**			**		*						
superiortemporal	2	40				* X											
superiortemporal	2	43			**	** X											**

Table S4A. First tile GLM analysis for all gray matter electrodes that showed n-since-last-click as a significant predictor. Each column (starting from column 4) shows a separate predictor. Yellow rows indicate the example electrodes in **Figure 4E-H** (first row) and **Figure S5** (second row).*: p<0.01. **: p<0.001. X: most significant predictor.

Region	Sub	Channel	match	n-since-pair* match	n-since-last-click	first-click	n-times-seen	next-match	RT	board-size	x-position	y-position	distance	animal	food	person	vehicle
Hippocampus	6	6			*		* X										
bankssts	16	41			*									*		** X	
bankssts	16	42			*									*	*	** X	
entorhinal	6	27	*		* X												
fusiform	2	13			* X												
fusiform	3	11			*	*			**					** X			
fusiform	6	11			** X	*											*
fusiform	8	63			**	** X											
inferiorparietal	3	71			** X	**			**							*	
inferiorparietal	18	150			** X	**				**		*					
inferiorparietal	18	151			** X	**					*					*	
inferiorparietal	18	152			** X												
inferiortemporal	7	38	*		*				** X		*						
inferiortemporal	18	143	*		**	** X											
inferiortemporal	18	144			** X	*											
insula	18	27	**	**	** X												
insula	18	28	**	**	** X												
insula	18	29	**	**	** X												
insula	18	34			**					** X							
lateralorbitofrontal	15	22			** X	**		*	*			*					
lateralorbitofrontal	15	73			*				**							** X	
lateralorbitofrontal	18	25	*		*	* X				*							
lateralorbitofrontal	18	26	**	**	**	** X				*							
middletemporal	11	45		*	* X			*									
middletemporal	14	48			* X												
middletemporal	16	24			*				*					** X			
middletemporal	18	134			*	* X											
parahippocampal	6	8			**												** X
parahippocampal	6	9			**							**					** X
parahippocampal	10	8			* X												
parsopercularis	8	22			** X	**			**					*			
parsopercularis	8	23			**	** X			**							**	
parsopercularis	11	78			*	** X		*						*			*
parsopercularis	18	32			*	** X											
parstriangularis	10	59			** X												
postcentral	12	39			*				* X			*					
postcentral	12	49			** X												
precentral	15	15			*	** X			**								
precentral	15	16			**	** X				**							
rostralmiddlefrontal	8	24			**	** X			**							*	
superiorfrontal	12	6			**				** X								
superiorparietal	3	111			*				*		** X						
superiorparietal	3	112			*				* X								
superiortemporal	2	44			*	** X											
supramarginal	2	37			*				** X				**				

Table S4B. First tile GLM analysis for all white matter electrodes that showed n-since-last-click as a significant predictor. Each column (starting from column 4) shows a separate predictor. Yellow row indicates the example electrode in **FigureS4**. *: p<0.01. **: p<0.001. X: most significant predictor.

Region	Sub	Channel	match	n-since-pair* match	n-since-last-click	first-click	n-times-seen	next-match	RT	board-size	x-position	y-position	distance	animal	food	person	vehicle
caudalanteriorcingulate	8	21	**		** X	**			**								
fusiform	3	12			**				**					** X		**	
fusiform	3	28			** X	**			**				*			**	
fusiform	6	12			*					*				** X	*	**	
fusiform	6	53			** X											**	**
fusiform	18	138			**	** X				**	**					*	
fusiform	18	139			**	** X				*	*						
fusiform	18	140			**	** X			**	**	*						
fusiform	18	141			**	** X				*							
fusiform	18	142	*		**	** X				*							
inferiortemporal	7	39			**	*			** X		*						
inferiortemporal	7	40			*										**	** X	
inferiortemporal	7	41			*				**					** X	**	**	
lateralorbitofrontal	6	66			* X												
lateralorbitofrontal	6	67			**				** X								
lateralorbitofrontal	6	68			*												** X
lateralorbitofrontal	13	31			* X				*								
lateralorbitofrontal	15	21			** X	**			*								
lateralorbitofrontal	15	23			** X	*											
lateralorbitofrontal	15	74	*		**										*	** X	
lateralorbitofrontal	15	75			* X												
middletemporal	5	66			* X												
parahippocampal	6	50	*		** X												
parsorbitalis	15	76	** X		*												
parstriangularis	4	49	** X		*				*								
precentral	4	59	* X		*												
rostralmiddlefrontal	15	3			** X	**											
superiorparietal	3	23			** X	**			*								
superiorparietal	3	70			** X	**											
superiorparietal	3	72			** X	**			*								
superiorparietal	3	73			** X	**			**		*						
superiortemporal	2	43			**	** X											**

Table S5A. First tile GLM analysis for all gray matter electrodes that showed match as a significant predictor. Each column (starting from column 4) shows a separate predictor. Yellow rows indicate the example electrodes in **Figure 5** (first row), **Figure S7** (first row), and **Figure S8** (second row).*: p<0.01. **: p<0.001. X: most significant predictor.

Region	Subject	Channel	match	n-since-pair* match	n-since-last-click	first-click	n-times-seen	next-match	RT	board-size	x-position	y-position	distance	animal	food	person	vehicle
Hippocampus	2	47	* X														
Hippocampus	16	28	** X														
bankssts	4	36	* X												*		
entorhinal	6	27	*		* X												
fusiform	6	10	*														* X
inferiortemporal	7	18	** X														
inferiortemporal	7	38	*		*				** X		*						
inferiortemporal	18	143	*		**	** X											
insula	18	27	**	**	** X												
insula	18	28	**	**	** X												
insula	18	29	**	**	** X												
insula	19	55	* X														
lateralorbitofrontal	4	39	* X											*			
lateralorbitofrontal	4	42	* X														
lateralorbitofrontal	4	43	** X														
lateralorbitofrontal	4	45	** X								*						
lateralorbitofrontal	10	46	** X														
lateralorbitofrontal	18	25	*		*	* X				*							
lateralorbitofrontal	18	26	**	**	**	** X				*							
middletemporal	2	52	** X	**													
middletemporal	8	37	*				*									** X	
middletemporal	13	45	**						*			*	** X				
middletemporal	18	109	* X														
middletemporal	18	110	** X	*		*										*	
parahippocampal	10	7	** X	*													
parsopercularis	6	82	** X					*	*								
parsopercularis	6	83	** X	*													
parsopercularis	10	57	** X							*							
precentral	19	106	** X	*												*	
precuneus	1	77	** X	*													
rostralanteriorcingulate	9	34	** X														
supramarginal	2	32	** X	**		*	**		**				*				

Table S5B. First tile GLM analysis for all white matter electrodes that showed match as a significant predictor. Each column (starting from column 4) shows a separate predictor. Yellow row indicates the example electrode in **Figure S6**. *: p<0.01. **: p<0.001. X: most significant predictor.

Region	Sub	Channel	match	n-since-pair* match	n-since-last-click	first-click	n-times-seen	next-match	RT	board-size	x-position	y-position	distance	animal	food	person	vehicle
caudalanteriorcingulate	8	21	**		** X	**			**								
entorhinal	10	19	** X														
fusiform	18	142	*		**	** X				*							
inferiortemporal	6	57	** X														
inferiortemporal	7	19	* X														
inferiortemporal	7	63	* X														
lateralorbitofrontal	4	41	** X														
lateralorbitofrontal	4	44	* X														
lateralorbitofrontal	10	55	** X	**			*										
lateralorbitofrontal	14	34	** X														
lateralorbitofrontal	14	36	** X	*			*										*
lateralorbitofrontal	15	74	*		**										*	** X	
lingual	11	60	*								**	*		**		** X	
medialorbitofrontal	11	63	** X					*									
middletemporal	9	24	** X														
middletemporal	13	44	*						*			*	** X				
parahippocampal	6	50	*		** X												
parsopercularis	6	81	** X	**													
parsorbitalis	15	76	** X		*												
parstriangularis	4	49	** X		*				*								
parstriangularis	7	82	** X	*													
parstriangularis	7	84	** X	**													
precentral	4	55	** X														
precentral	4	56	** X														
precentral	4	57	** X	*													
precentral	4	58	** X														
precentral	4	59	* X		*												
superiorparietal	3	20	*			*				* X							
superiortemporal	6	19	*					*			* X		*				
supramarginal	2	31	** X	**					*								

Table S6A. First tile GLM analysis for all gray matter electrodes that showed n-since-pair*match as a significant predictor. Each column (starting from column 4) shows a separate predictor. Yellow row indicates the example electrode in **Figure 6**.*: p<0.01. **: p<0.001. X: most significant predictor.

Region	Sub	Channel	match	n-since-pair* match	n-since-last-click	first-click	n-times-seen	next-match	RT	board-size	x-position	y-position	distance	animal	food	person	vehicle
insula	18	27	**	**	** X												
insula	18	28	**	**	** X												
insula	18	29	**	**	** X												
lateralorbitofrontal	18	3		* X													
lateralorbitofrontal	18	6		*		** X				**							
lateralorbitofrontal	18	26	**	**	**	** X				*							
medialorbitofrontal	18	2		* X													
middletemporal	2	52	** X	**													
middletemporal	11	45		*	* X			*									
middletemporal	18	110	** X	*		*										*	
parahippocampal	10	7	** X	*													
parsopercularis	6	83	** X	*													
precentral	19	106	** X	*												*	
precuneus	1	77	** X	*													
supramarginal	2	32	** X	**		*	**		**				*				

Table S6B. First tile GLM analysis for all white matter electrodes that showed n-since-pair*match as a significant predictor. Each column (starting from column 4) shows a separate predictor. Yellow row indicates the example electrode in **Figure S9**. *: p<0.01. **: p<0.001. X: most significant predictor.

Region	Sub	Channel	match	n-since-pair* match	n-since-last-click	first-click	n-times-seen	next-match	RT	board-size	x-position	y-position	distance	animal	food	person	vehicle
lateralorbitofrontal	10	55	** X	**			*										
lateralorbitofrontal	14	6		** X									*				
lateralorbitofrontal	14	36	** X	*			*										*
middletemporal	18	60		*						* X		*					
parsopercularis	6	81	** X	**													
parstriangularis	7	82	** X	*													
parstriangularis	7	84	** X	**													
precentral	4	57	** X	*													
supramarginal	2	31	** X	**					*								

Table S7A. Second tile GLM analysis for all gray matter electrodes that showed first-click as a significant predictor. Each column (starting from column 4) shows a separate predictor. *: p<0.01. **: p<0.001. X: most significant predictor.

Region	Sub	Channel	match	n-since-last-click	first-click	n-times-seen	next-match	RT	board-size	x-position	y-position	distance	animal	food	person	vehicle
Amygdala	10	10			* X											
Hippocampus	18	104	** X		**											
bankssts	18	131	*		*			** X	*							
fusiform	3	11		*	*								** X			
fusiform	10	37			*											** X
insula	18	27	** X		**	*		*								
insula	18	28	** X		*	*										
lateraloccipital	20	4			* X											
lateraloccipital	20	5			** X											
lateralorbitofrontal	15	22	*	**	**		*							**		** X
lateralorbitofrontal	18	5			* X				*							
lateralorbitofrontal	18	25	**		** X	**		**								
lateralorbitofrontal	18	26	**	*	** X	**		**								
lingual	1	12	*		*						** X			*		
parahippocampal	9	27			*				** X							
parsopercularis	8	22	**	**	**			** X	**				**			
parsopercularis	8	23	**		**			** X	**							
postcentral	20	83			* X					*						
postcentral	20	84		*	* X											
precentral	18	40			* X	*						*				
precentral	12	24	*	*	* X											
precuneus	1	77			*		** X									
rostralmiddlefrontal	8	24	** X	*	**			**								
superiortemporal	18	119			* X						*					

Table S7B. Second tile GLM analysis for all white matter electrodes that showed first-click as a significant predictor. Each column (starting from column 4) shows a separate predictor. *: p<0.01. **: p<0.001. X: most significant predictor.

Region	Sub	Channel	match	n-since-last-click	first-click	n-times-seen	next-match	RT	board-size	x-position	y-position	distance	animal	food	person	vehicle
caudalanteriorcingulate	8	21	**	**	*			** X								
fusiform	18	138	** X	**	*				**	*					*	
inferiorparietal	20	15			** X											
lateralorbitofrontal	6	68		*	** X	*										
lateralorbitofrontal	15	23		*	**											** X
lateralorbitofrontal	18	24	**	*	** X	*										
parstriangularis	16	7			** X											
parstriangularis	16	9			** X											
posteriorcingulate	20	123			** X			*								
precentral	4	54			* X											
precentral	4	57			*		* X									
precentral	4	58			*		** X									

Table S8A. Second tile GLM analysis for all gray matter electrodes that showed n-since-last-click as a significant predictor. Each column (starting from column 4) shows a separate predictor. Yellow row indicates the example electrode in **Figure S10**. *: p<0.01. **: p<0.001. X: most significant predictor.

Region	Sub	Channel	match	n-since-last-click	first-click	n-times-seen	next-match	RT	board-size	x-position	y-position	distance	animal	food	person	vehicle
fusiform	3	11		*	*								** X			
lateralorbitofrontal	122	46		* X												
lateralorbitofrontal	15	22	*	**	**		*							**		** X
lateralorbitofrontal	18	9	** X	*				**	*							
lateralorbitofrontal	18	26	**	*	** X	**		**								
parsopercularis	8	22	**	**	**			** X	**				**			
postcentral	20	84		*	* X											
precentral	12	24	*	*	* X											
rostralmiddlefrontal	8	24	** X	*	**			**								

Table S8B. Second tile GLM analysis for all white matter electrodes that showed n-since-last-click as a significant predictor. Each column (starting from column 4) shows a separate predictor. *: p<0.01. **: p<0.001. X: most significant predictor.

Region	Sub	Channel	match	n-since-last-click	first-click	n-times-seen	next-match	RT	board-size	x-position	y-position	distance	animal	food	person	vehicle
caudalanteriorcingulate	8	21	**	**	*			** X								
caudalmiddlefrontal	3	90		** X			*									
fusiform	3	28		**				*							** X	
fusiform	6	12	**	**									** X	*	*	
fusiform	6	53		*				**							** X	*
fusiform	18	138	** X	**	*				**	*					*	
fusiform	18	139	** X	**				*		*						
fusiform	18	140	** X	*				**		**						
fusiform	18	141	** X	**				**		*						
lateralorbitofrontal	6	68		*	** X	*										
lateralorbitofrontal	15	21	** X	*												
lateralorbitofrontal	15	23		*	**											** X
lateralorbitofrontal	15	74		*				** X							*	
lateralorbitofrontal	18	24	**	*	** X	*										
middletemporal	7	10		* X												
middletemporal	7	66		*										* X	*	
middletemporal	7	67	* X	*							*					
parahippocampal	6	50	*	** X												
parsorbitalis	6	71		* X												
parsorbitalis	15	76		*				*								** X
parstriangularis	2	28		* X												
parstriangularis	2	29		*												* X
parstriangularis	7	83	** X	*			*									
superiorparietal	3	72	** X	*					*						*	

Table S9A. Second tile GLM analysis for all gray matter electrodes that showed match as a significant predictor. Each column (starting from column 4) shows a separate predictor. Yellow row indicates the example electrode in **Figure 7** and **Figure S9**. *: p<0.01. **: p<0.001. X: most significant predictor.

Region	Sub	Channel	match	n-since-last-click	first-click	n-times-seen	next-match	RT	board-size	x-position	y-position	distance	animal	food	person	vehicle
Amygdala	6	16	*				* X									
Amygdala	7	4	** X													
Amygdala	8	51	** X													
Hippocampus	2	47	* X			*										
Hippocampus	16	28	** X													
Hippocampus	18	102	** X													
Hippocampus	18	103	** X													
Hippocampus	18	104	** X		**											
Hippocampus	18	105	** X													
bankssts	16	42	*											* X		
bankssts	18	131	*		*			** X	*							
bankssts	18	132	** X					**	*							
caudalmiddlefrontal	13	69	** X							*						
caudalmiddlefrontal	13	73	** X													
entorhinal	19	2	*									* X				
inferiorparietal	3	60	** X						*							
inferiorparietal	3	71	** X					**					*		**	
inferiorparietal	16	62	** X						*							
inferiorparietal	16	63	** X													
inferiortemporal	1	65	* X													
inferiortemporal	1	66	*					*							*	* X
inferiortemporal	7	21	** X													
inferiortemporal	7	37	* X					*								
inferiortemporal	7	38	** X					**								
insula	3	50	** X													
insula	6	77	** X					*								
insula	7	79	** X													
insula	7	80	** X													
insula	18	27	** X		**	*		*								
insula	18	28	** X		*	*										
insula	18	29	** X													
insula	18	44	** X													
insula	18	45	** X													
insula	19	55	** X													
insula	19	104	* X					*								
insula	20	151	* X													
lateraloccipital	16	81	*					** X								
lateralorbitofrontal	4	39	** X													
lateralorbitofrontal	4	43	** X													
lateralorbitofrontal	4	45	** X													
lateralorbitofrontal	10	40	** X													
lateralorbitofrontal	10	43	** X													
lateralorbitofrontal	10	46	** X													

Table S9A continued...

lateralorbitofrontal	13	28	** X													
lateralorbitofrontal	13	29	** X				*									
lateralorbitofrontal	13	30	** X				**									
lateralorbitofrontal	15	22	*	**	**		*							**		** X
lateralorbitofrontal	18	3	** X					**			*					
lateralorbitofrontal	18	7	** X						**							
lateralorbitofrontal	18	8	** X					**	**							
lateralorbitofrontal	18	9	** X	*				**	*							
lateralorbitofrontal	18	20	** X						*							
lateralorbitofrontal	18	21	** X													
lateralorbitofrontal	18	22	** X											*		
lateralorbitofrontal	18	25	**		** X	**		**								
lateralorbitofrontal	18	26	**	*	** X	**		**								
lateralorbitofrontal	19	41	* X													
lateralorbitofrontal	19	54	* X													
lingual	1	12	*		*						** X			*		
medialorbitofrontal	18	2	** X					**	**							
medialorbitofrontal	18	18	** X													
medialorbitofrontal	18	19	** X						*							
middletemporal	1	60	** X								*					
middletemporal	2	52	** X													
middletemporal	9	32	** X													
middletemporal	13	19	* X													
middletemporal	13	45	** X													
middletemporal	16	22	* X													
middletemporal	16	23	* X													
middletemporal	16	24	* X													
middletemporal	18	108	** X													
middletemporal	18	109	** X													
middletemporal	18	133	** X						**		**					
middletemporal	18	134	** X								**					
middletemporal	18	135	** X						**		**					
middletemporal	18	148	* X													
parahippocampal	6	8	**										*	**	*	** X
parahippocampal	6	9	*										*			** X

Table S9A continued ...

parsopercularis	6	78	** X					*		**		**				
parsopercularis	8	22	**	**	**			** X	**				**			
parsopercularis	8	23	**		**			** X	**							
parsopercularis	18	30	** X			*			*							
parsopercularis	18	32	**					** X	*							
parsopercularis	20	50	* X													
parstriangularis	2	25	** X													
parstriangularis	6	74	** X					**								
parstriangularis	6	75	** X					**								
parstriangularis	10	59	** X													
parstriangularis	18	11	* X													
parstriangularis	18	12	** X					**	*							
parstriangularis	18	13	** X									*				
parstriangularis	18	14	** X					**	*							
postcentral	18	35	** X													
postcentral	12	39	* X													
posteriorcingulate	20	73	* X			*										
precentral	122	32	* X			*										
precentral	122	33	** X													
precentral	15	16	** X							*						
precentral	16	50	** X													
precentral	16	53	** X													
precentral	18	36	** X										*			
precentral	12	24	*	*	* X											
rostralanteriorcingulate	9	34	** X													
rostralmiddlefrontal	8	24	** X	*	**			**								
superiorfrontal	19	175	** X					*								
superiorfrontal	12	6	*					** X								
superiorparietal	16	61	** X					*	*							
superiorparietal	20	129	** X													
superiorparietal	20	130	** X													*
supramarginal	2	37	* X													
supramarginal	16	64	** X													
supramarginal	16	65	** X													

Table S9B. Second tile GLM analysis for all white matter electrodes that showed match as a significant predictor. Each column (starting from column 4) shows a separate predictor. Yellow row indicates the example electrode in **Figure S11**. *: p<0.01. **: p<0.001. X: most significant predictor.

Region	Sub	Channel	match	n-since-last-click	first-click	n-times-seen	next-match	RT	board-size	x-position	y-position	distance	animal	food	person	vehicle
caudalanteriorcingulate	8	21	**	**	*			** X								
fusiform	6	12	**	**									** X	*	*	
fusiform	7	5	** X													
fusiform	7	6	* X													
fusiform	18	106	** X													
fusiform	18	138	** X	**	*				**	*					*	
fusiform	18	139	** X	**				*		*						
fusiform	18	140	** X	*				**		**						
fusiform	18	141	** X	**				**		*						
inferiorparietal	3	59	** X													
inferiortemporal	1	69	** X				*					*				
inferiortemporal	1	81	** X													
inferiortemporal	6	42	** X				*	**								
inferiortemporal	6	57	** X													
inferiortemporal	6	58	** X													
inferiortemporal	6	59	* X													
inferiortemporal	6	60	*					* X								
inferiortemporal	7	39	** X					**								
inferiortemporal	18	107	** X													
inferiortemporal	18	147	* X						*							
insula	3	49	** X													
lateralorbitofrontal	4	40	** X													
lateralorbitofrontal	4	41	** X													
lateralorbitofrontal	4	44	** X													
lateralorbitofrontal	6	64	** X								*					
lateralorbitofrontal	6	66	** X													
lateralorbitofrontal	6	67	** X													
lateralorbitofrontal	10	55	** X				**									
lateralorbitofrontal	13	32	*					** X				*				
lateralorbitofrontal	15	21	** X	*												
lateralorbitofrontal	18	23	** X													
lateralorbitofrontal	18	24	**	*	** X	*										
lingual	11	60	*										** X	**	**	
medialorbitofrontal	11	63	** X													
middletemporal	5	9	* X													
middletemporal	7	65	*					*					*	* X		
middletemporal	7	67	* X	*							*					
middletemporal	13	44	** X													
paracentral	3	106	*					*	** X							
parahippocampal	1	10	**										** X	**	**	
parahippocampal	6	50	*	** X												
parsopercularis	6	79	** X									*				
parsopercularis	6	80	** X					*		*						
parsopercularis	6	81	** X					*								
parsopercularis	13	67	** X													
parsorbitalis	5	54	** X													
parstriangularis	4	49	* X													
parstriangularis	7	82	** X				*				*					
parstriangularis	7	83	** X	*			*									
parstriangularis	7	84	** X									*				
pericalcarine	20	1	* X													
precentral	3	54	* X				*									
precentral	3	55	** X				*						*	**		
precentral	4	55	** X					*								
rostralmiddlefrontal	3	80	* X													
rostralmiddlefrontal	15	3	** X													
superiorfrontal	19	173	** X													
superiorfrontal	19	174	** X													
superiorfrontal	19	183	** X													
superiorparietal	3	21	*					** X								
superiorparietal	3	70	* X				*									
superiorparietal	3	72	** X	*					*						*	
superiorparietal	3	73	* X													
superiortemporal	2	43	* X													
supramarginal	2	31	** X				*	**								
transversetemporal	8	10	** X					*								